

Wave and Wind Energy

Salina, Italy

Author : Dimitri Al. Katsaprakakis (Hellenic Mediterranean University)

Reviewers: Marie Angot (3E), Carlos Guerrero (3E)

Date : 27/02/2020

CLEAN ENERGY FOR EU ISLANDS

Secretariat • Rue d'Arlon 63, BE-1000 Brussels
Phone +32 2 400 10 67 • E-mail info@euislands.eu • Website euislands.eu

DISCLAIMER

This study has been prepared for the European Commission by the Clean Energy for EU Islands Secretariat. It reflects the views of the authors only. These views have neither been adopted nor in any way approved by the Commission and should not be relied upon as a statement of the Commission's or DG ENER's views. The results of this study do not bind the Commission in any way. The Commission does not guarantee the accuracy of the data included in the study. Neither the Commission nor any person acting on the Commission's behalf may be held responsible for the use which may be made of the information contained therein.

This document is based on an application submitted by an island-related organization to a Call for 'Project specific support' organized as part of the Clean Energy for EU Island Secretariat, and entered into solely between the Clean Energy for EU Island Secretariat and the island-related organization for whom it was drafted, and no third-party beneficiaries are created hereby. This document may be communicated or copied to third parties, and third parties may make use of this document without the prior written consent of the Clean Energy for EU Island Secretariat and/or its author. The Clean Energy for EU Island Secretariat and the author will not be liable to any parties (the island-related organization or third-parties) for services rendered to the island-related organization, or for the consequences of the use by the island-related organization or a third party of this document.

EUROPEAN COMMISSION

Directorate-General for Energy
Directorate B — Internal Energy Market
Unit B2 — Wholesale markets; electricity & gas
Contact: Nicole Versijp
E-mail: Nicole.Versijp@ec.europa.eu
European Commission

Table of Contents

The Clean Energy for EU Islands Secretariat	2
Who we are	2
Acknowledgments	3
Preface	4
Scope of this report	4
1. The island of Salina	5
Location	5
Existing situation regarding energy consumption and production	5
The area of interest	3
2. The available wind potential	4
The available wind potential	4
The available sea bed	7
Alternative investigated offshore wind parks scenarios	9
3. Wave potential	16
Introduction	16
Theoretical basis of wave energy	16
The global wave potential	18
Wave potential in Mediterranean Sea	21
Wave potential in the Italian coast and in the Salina Island	24
4. Wave Energy Converters	31
Classification versus the installation location	31
Classification versus the device size and the directional wave characteristics	32
Attenuators	32
Point absorbers	33
Terminators	33
Classification versus the working principle	34
Pressure differential devices	34
Floating structures	37
Overtopping systems	40
Impact devices	41
Conclusions	43
References	44

The Clean Energy for EU Islands Secretariat

Who we are

The launch of the Clean Energy for EU Islands Initiative in May 2017 underlines the European Union's intent to accelerate the clean energy transition on Europe's more than 1,400 inhabited islands. The initiative aims to reduce the dependency of European islands on energy imports by making better use of their own renewable energy sources and embracing modern and innovative energy systems. As a support to the launch of the initiative, the Clean Energy for EU Islands Secretariat was set up to act as a platform of exchange for island stakeholders and to provide dedicated capacity building and technical advisory services.

The Clean Energy for EU Islands Secretariat supports islands in their clean energy transition in the following ways:

- It provides technical and methodological support to islands to develop clean energy strategies and individual clean energy projects.
- It co-organises workshops and webinars to build capacity in island communities on financing, renewable technologies, community engagement, etc. to empower them in their transition process.
- It creates a network at a European level in which islands can share their stories, learn from each other, and build a European island movement.

The Clean Energy for EU Islands Secretariat provides a link between the clean energy transition stories of EU islands and the wider European community, in particular the European Commission.

Acknowledgments

T Special thanks are owed to the following contributors of this study:

- to 3E (<http://www.3e.eu/>), Partner of the Secretariat, for the supply of the wind and the ambient temperature data
- to Hellenic Centre of Marine Research, and particularly to Dr. Takvor Soukissian, for the supply of the wave potential data

Preface

Scope of this report

This report has been accomplished within the frame of the first open call announced by the European Commission's Secretariat on "Clean Energy for E.U. Islands" (Secretariat) for the support of insular communities – initiatives in the European Continent on specific projects regarding their energy transition from fossil fuels to renewable energy sources and rational use of energy. This report has been developed following the application submitted by the Agenzia Nazionale per l'Efficienza Energetica (ENEA – DUÉE SIST SUD), and approved by the Secretariat, for the island of Salina, Italy. According to the submitted application, the requested support should be focused on:

- the estimation of the available wind and wave potential at the north – west offshore area of Salina
- a description of the most technically mature and economically competitive technologies for electricity production from wave energy.

1. The island of Salina

Location

The island of Salina is located at the south of Italy, north of Sicily, as shown in Figure 1. It is a small island with a total area of 26.8 km² and a permanent population of 2,598 inhabitants [1]. The distance of the southern settlement Rinella in Salina from Palermo (Sicily) is 73 n.m.



Figure 1: The island of Salina and its location with regard to Sicily.

Existing situation regarding energy consumption and production

The existing energy consumption in the island of Salina is classified in the following forms:

- electricity, for the following uses:
 - municipal buildings and residential sector
 - tertiary sector (essentially tourism)
 - public lighting
 - primary and secondary sector
- LPG, with the following discrete uses
 - tertiary sector (essentially tourism)
 - residential sector
- diesel oil, with the following discrete uses:
 - primary and secondary sector (agriculture, fishing, service supply, industry)
 - transportation on the island
 - transportation from and to the island
- gasoline, exclusively for the transportation sector
- thermal energy from solar collectors, for hot water production in residential and public buildings.

The annual energy consumption in Salina Island is analysed in Table 1.

Table 1: Annual energy consumption analysis in Salina island.

Energy Consumption Category		Residential and public buildings	Primary and secondary sector (agriculture, fishing, service supply, industry)	Tertiary sector (including tourism)	Transportation on island	Final or primary energy consumption on island	Transportation from and to the island	Final or primary energy total consumption
Electricity (MWh)	Final	4,067	730	3,363		8,160		8,160
	Primary	13,119	2,355	10,848		26,322		26,322
Fossil fuels primary energy (MWh)	LPG	1,286		904		2,190		2,190
	Diesel oil		1,284		6,327	7,611	61,028	68,639
	Gasoline				6,827	6,827		6,827
Thermal solar panels substituting electricity (MWh)	Final thermal	9				9		9
	Primary	29				29		29
Total primary energy (MWh)		14,434	3,639	11,752	13,154	42,979	61,028	104,007

As seen in Table 1, the current annual electricity consumption in the island is 8,160 MWh. In a future approach, the energy needs in the transportation sector are going to be transferred to the electrical grid too, substituting the current diesel oil and gasoline consumption with electricity. Additionally, in an effort to eliminate the fossil fuel consumption onshore, the current LPG consumption in residential and public buildings and in tourist sector, most probably for cooking, can be also substituted with electricity. In order to proceed to an estimation of these future additional electricity consumptions, the following assumptions – parameters are introduced:

- lower calorific value of diesel oil H_{ud} : 10.25 kWh/L
- lower calorific value of gasoline H_{ug} : 8.90 kWh/L
- lower calorific value of LPG H_{LPG} : 12.64 kWh/kg
- initial to primary energy conversion factor for diesel oil f_d : 1.10 [2]
- initial to primary energy conversion factor for gasoline f_g : 1.15 [2]
- initial to primary energy conversion factor for LPG f_{LPG} : 1.05 [2]
- average total efficiency of LPG cooking devices η_{LPG} : 0.90
- average total efficiency of electrical cooking devices η_{el} : 0.95
- average diesel oil or gasoline specific consumption for transportation v : 7 L/100 km
- average electricity specific consumption for transportation e : 20 kWh/100 km

Having the diesel oil, gasoline and LPG annual primary energy consumptions E_{pd} , E_{pg} and E_{LPG} respectively, the corresponding total annual volume and mass consumptions V_d , V_g and m_{LPG} respectively are calculated with the following relationships:

$$\begin{aligned} V_d &= \frac{E_{pd}}{H_{ud} \cdot f_d} \\ V_g &= \frac{E_{pg}}{H_{ug} \cdot f_g} \\ m_{LPG} &= \frac{E_{LPG}}{H_{LPG} \cdot f_{LPG}} \end{aligned} \quad (1)$$

It should be underlined that the diesel oil primary energy E_{pd} involved in this calculation refers only to the existing diesel oil consumption for the transportation sector, namely $E_{pd} = 6,327$ MWh. The existing diesel oil consumption in the secondary sector (agriculture, industry, fishing) is not included in this calculation.

The corresponding total electricity consumption E_t substituting the current diesel oil and gasoline consumption in the transportation sector, can now be calculated with the following relationship:

$$E_t = \frac{V_d + V_g}{v} \cdot e \quad (2)$$

Finally, the corresponding electricity consumption E_c substituting the current LPG primary energy consumption E_{LPG} is calculated with the following relationship:

$$E_c = \frac{E_{LPG} \cdot \eta_{LPG}}{\eta_{el}} \quad (3)$$

The data and the results of the above executed calculations are summarized in Table 2.

Table 2: Estimation of the additional electricity consumption, substituting the existing diesel oil and LPG consumption for transportation and cooking needs.

Energy source	Existing primary energy consumption (MWh)	Volume or mass consumption (L / kg)	Corresponding electricity consumption (MWh)
Diesel oil	6,327	561,153 L	1,603
Gasoline	6,827	667,775 L	1,908
LPG	2,190	165,009 kg	2,075
Total:			5,586

From the above analysis it is concluded that the transition of the transportation and the cooking needs coverage from diesel oil and LPG to electricity imposes a 68% increase of the current electricity annual consumption (8.160 MWh). The total new annual electricity consumption is formulated at 13.746 MWh.

The area of interest

Given the requirements of the submitted application by ENEA – DUEE SIST SUD, the area of interest for the development of offshore wind parks and electricity production projects from wave energy is located at the north – west coast of the island, between the settlements of Malfa and Pollara, as shown in Figure 2.



Figure 2: The area of interest for the development of offshore wind parks and electricity production projects from wave energy.

2. The available wind potential

The available wind potential

The available wind potential in the under consideration offshore area was estimated on the basis of wind potential data retrieved by the ERA-5 database of the European Centre for Medium-Range Weather Forecasts (ECMWF) for the period 2000 – 2018 [3]. The employed wind potential measurements were downloaded for the measurement point with geographical coordinates $38^{\circ} 38' 30''\text{N}$, $14^{\circ} 45' 56''\text{E}$. The location of this point with regard to the Salina Island is depicted in Figure 3. As shown in this figure, the measurement point is quite near to the under interest area, with a distance from the northwest cape of the island at 7.8 km.



Figure 3: Location of the ERA-5 measurement point with regard to the Salina Island.

According to the available long-term wind measurements (19-year period), the fluctuation versus time of the annual average wind velocity at the height of 100 m above sea level are presented in Figure 4.

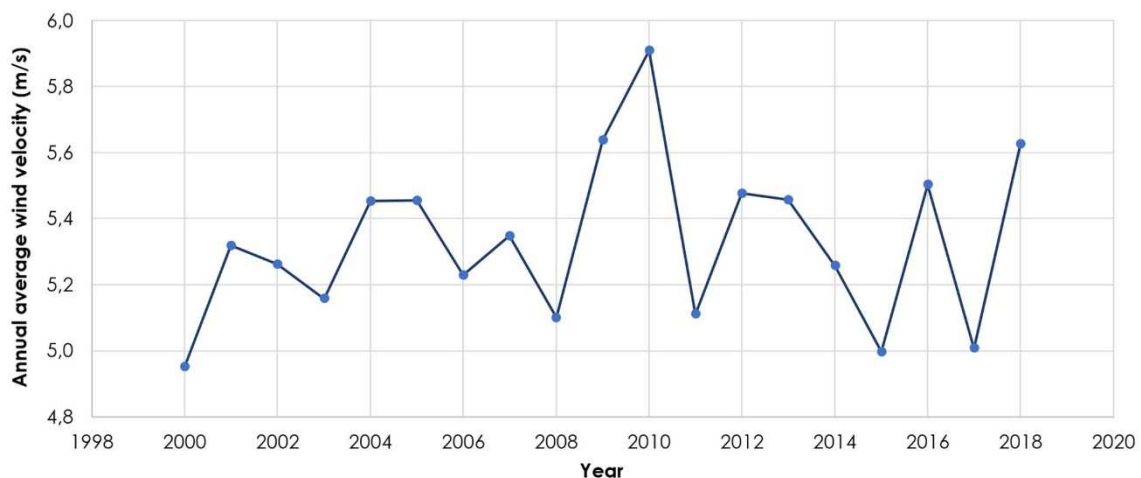


Figure 4: Fluctuation versus time of the annual average wind velocity at the wind potential measurement point and at 100 m height above sea level [3].

As seen in Figure 4, the annual average wind velocity ranges between roughly 4.9 m/s (in 2000) and 5.9 m/s in 2010 at 100 m height above sea level. Hence, at a first glance, it can be concluded that the specific geographical area has low wind potential. A closer look on the available wind potential is provided in Figure 5, where the annual fluctuation of the monthly average wind velocity is presented for three characteristic years of the available measurement period (2000 – 2018). These years are 2000, 2010 and 2012, namely the years with the minimum, the maximum and a moderate respectively annual average wind velocity.

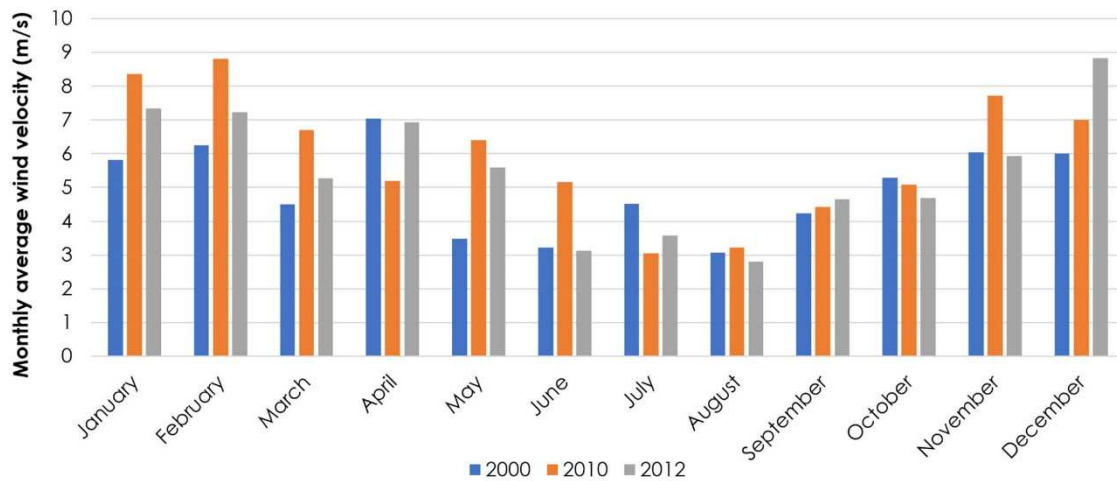


Figure 5: Annual fluctuation of the monthly average wind velocity for the years 2000, 2010 and 2012.

By observing Figure 5, we may conclude to the following remarks:

- The wind potential in the under interest area is maximized in winter and minimized in summer, while in spring and autumn it remains in moderate levels.
- All the examined years appear approximately the same annual fluctuation pattern for the monthly average wind velocity.
- The season which mainly affects and determines the level of the annual average wind velocity, and consequently the intensity of the available wind potential, is winter. This is clearly derived by realising that the monthly average wind velocity from July to October in 2010, namely of the year with the maximum annual average wind velocity, is either lower than or at the same level with the years 2000 and 2012. Yet, in 2010 the annual average wind velocity is higher than in the other two years because of the considerably higher available wind potential from November to March, with the exception of December for the year 2012.

Another closer insight in the available wind potential is provided in Figure 6, where the fluctuation of the wind velocity hourly average values for the two most recent integrated consecutive years, namely for 2017 and 2018, is plotted. As seen in this figure, the highest values are found mainly from January to March, namely during the winter period. During summer, due to the milder climate conditions, the wind velocity remains rather in low levels. This is certainly an unfavourable feature, with regard to the achievement of high RES penetration percentage and the approach of energy independency, given that during summer the electricity consumption is maximized due to the tourist activities. Hence, there is not a time coincidence between the power demand and the available wind potential. Finally, certain similarities are seen between the two years depicted in Figure 6, revealing the periodical attribute of wind potential in the under consideration area.

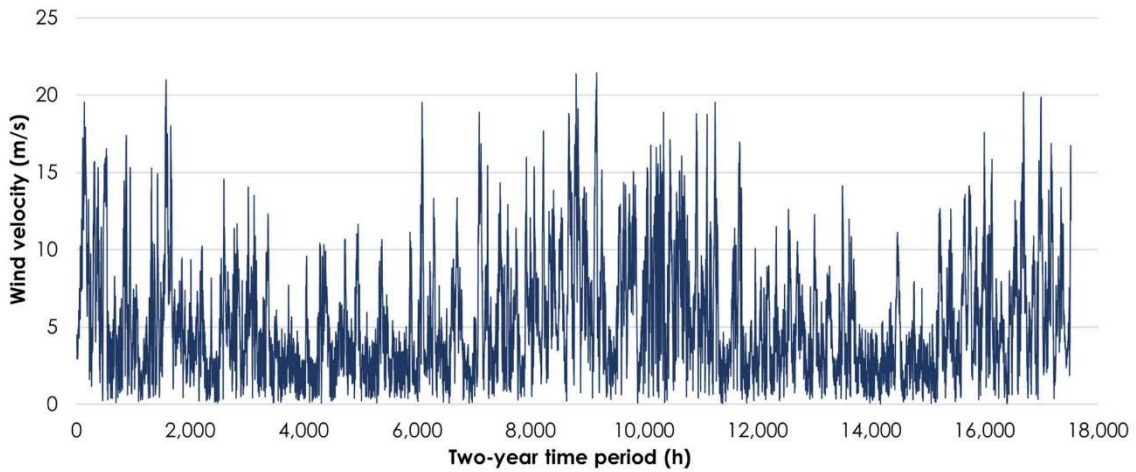


Figure 6: Fluctuation of hourly average wind velocity values versus time for the years 2017 and 2017 [3].

In Figure 7, the annual wind roses from the wind potential measurements gathered during 2000, 2010, 2012 and 2018 are presented. As seen in this figure, the wind prevailing directions in the under consideration location do not seem to change for the specific examined years, remaining mainly from the west and the west-northwest.

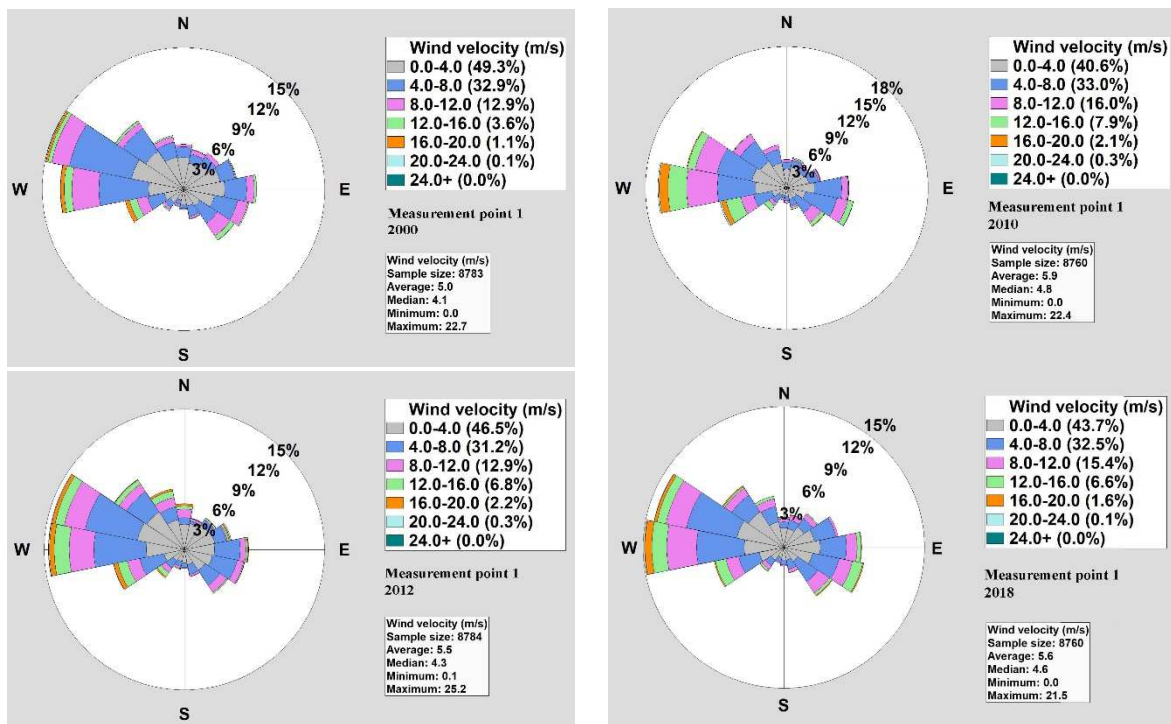
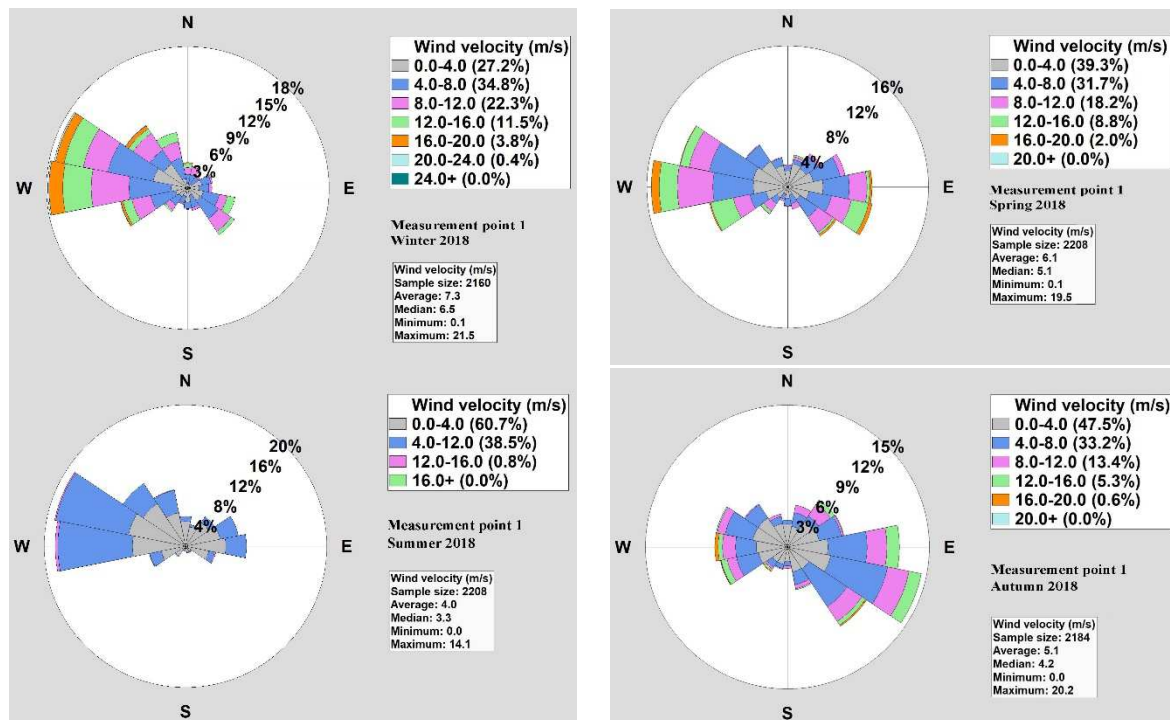


Figure 7: Annual wind roses for the years 2000, 2010, 2012 and 2018 for the under consideration measurement location [3].

Finally, in Figure 8, the seasonal wind roses are presented for the year 2018 and for the under consideration wind potential measurement location. In this figure it is seen that the prevailing wind blowing direction remain from the west and west-northwest from winter to summer. In autumn, the wind blowing direction changes and becomes from the east – southeast.

Additionally, in this figure it is clearly seen that the highest wind potential is available in winter, while it is remarkably reduced during summer.



The available sea bed

The available sea bed in the under interest area constitutes also a critical factor for the installation of offshore wind parks. Wind turbines can be relatively easily founded with conventional and widely implemented techniques on depths up to 50 m. In case of deeper sea beds, alternative techniques of floating wind turbines should be used with significantly increasing difficulties and set-up costs.

Salina Island is a volcanic island, with intensive land morphology and abrupt slopes. Obviously, the on-shore land morphology is maintained also underwater. A general 3D view of the land and the sea bed morphology in Salina Island is given in Figure 9 [4]. This view is taken from the north-west side of the land, in order to depict the under interest area.

A more detailed approach is given in Figure 10. In this Figure, the depth profile is plotted versus the distance from the coastline for two specific linear routes at the north-west coast of the island. It is seen that, despite the intensive land morphology, there is one location, at the west shore of the island, with relatively shallow sea. Unlike this route, the depth profile presented in the lower graph exhibits quite intensive slope. This depth profile is met for the whole island's coastline, as observed in both top-view graphs presented in Figure 10. In any case, for the route designated in the upper graph in Figure 10, it is shown that the depth of 50 m is met for distance longer than 700 m from the coastline. Given also the small size of the island and, sensibly, the small number of wind turbines required to approach energy independency (logically not more than 4-5 wind turbines of 3 MW each), it seems that this location provides enough space for the installation of offshore wind parks, to adequately meet the current and the future electricity needs on the island.

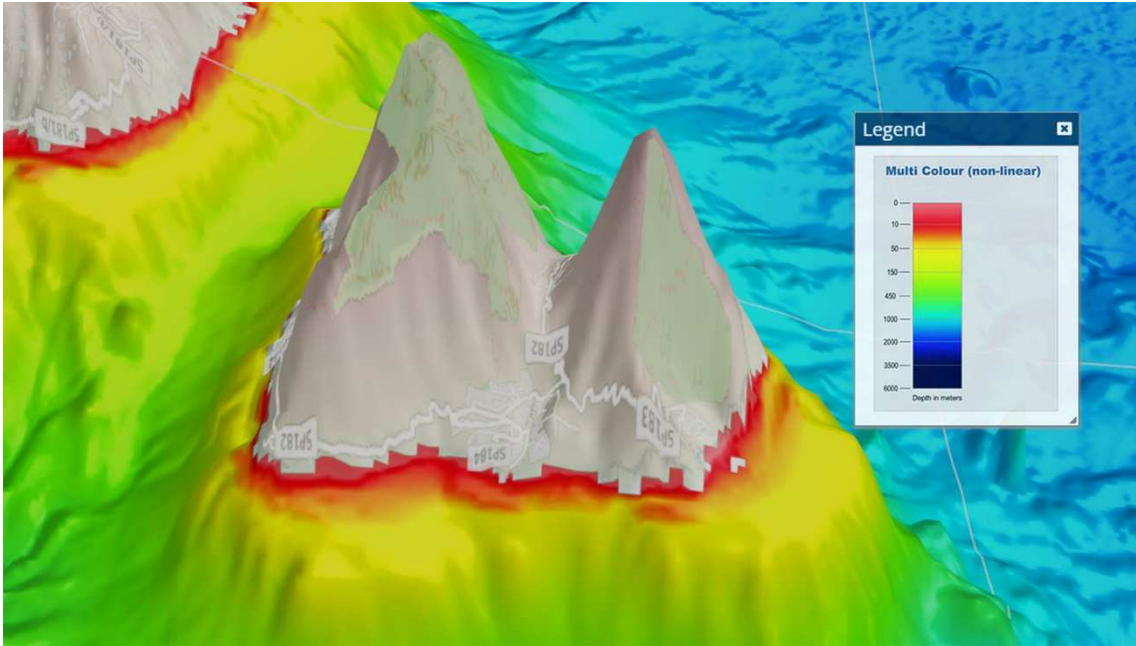


Figure 9: General 3D view of the land and sea bed morphology in Salina Island [4].

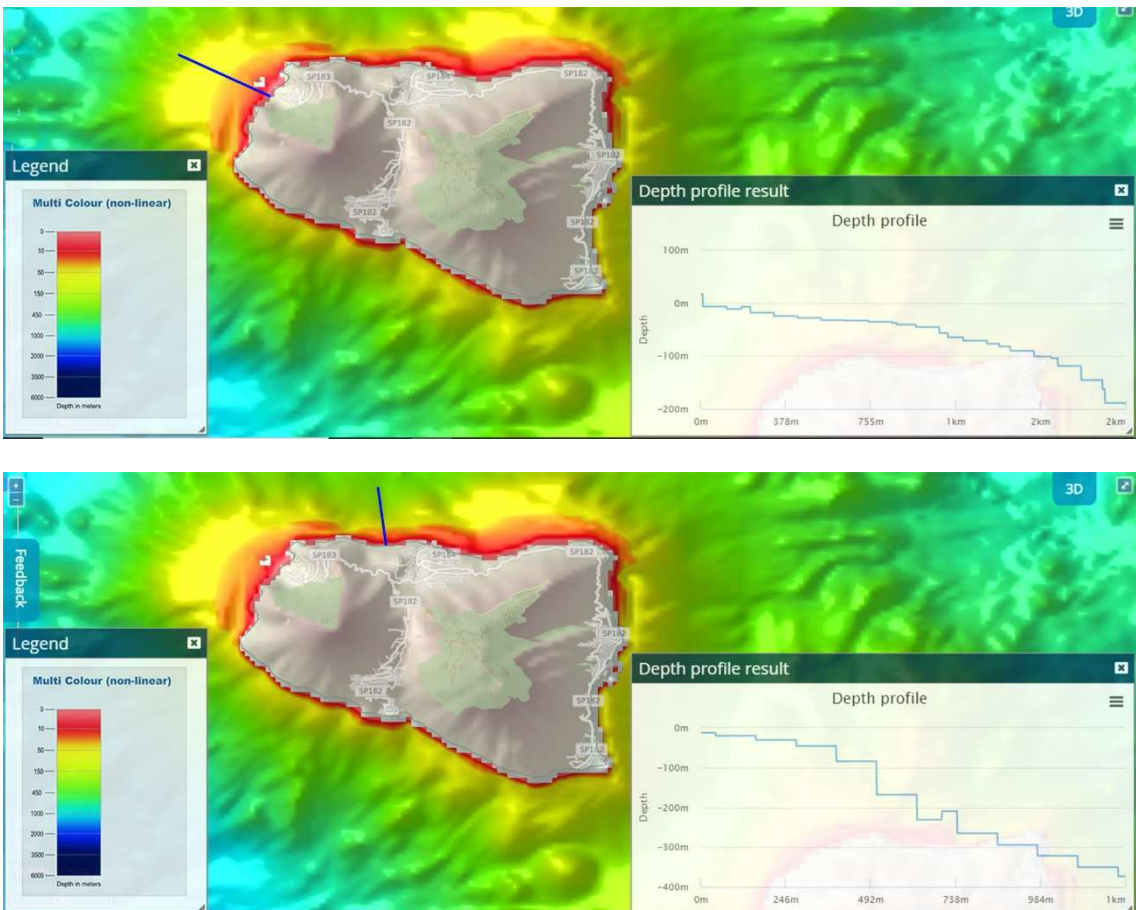


Figure 10: Depth profiles versus the distance from the coastline for two linear routes [4].

Alternative investigated offshore wind parks scenarios

For the purpose of this work, two alternative dimensioning and siting scenarios for offshore wind parks are investigated. Both of them are sited at the north-west coast of the island, at the favourable area indicated in Figure 10. The main difference between the two scenarios comes from the employed wind turbine model. In the first one, a 3.45 MW, Class IEC IB / IEC IIA wind turbine model, with a rotor's diameter of 117 m is introduced. In the second one, a 5 MW, Class IEC IIB wind turbine model, with a rotor's diameter of 126 m is used. The common goal of both investigated scenarios is the siting and the dimensioning of the wind park, so as the current and the future expecting annual electricity consumption in the island will be covered.

The available wind potential data and the digitized map of the island were introduced in WAsP software application for the development of the wind potential map at the height of 100 m above sea level. In the first investigated scenario, three wind turbines of 3 MW each were site as shown in Figure 11, on an annual average wind velocity background.

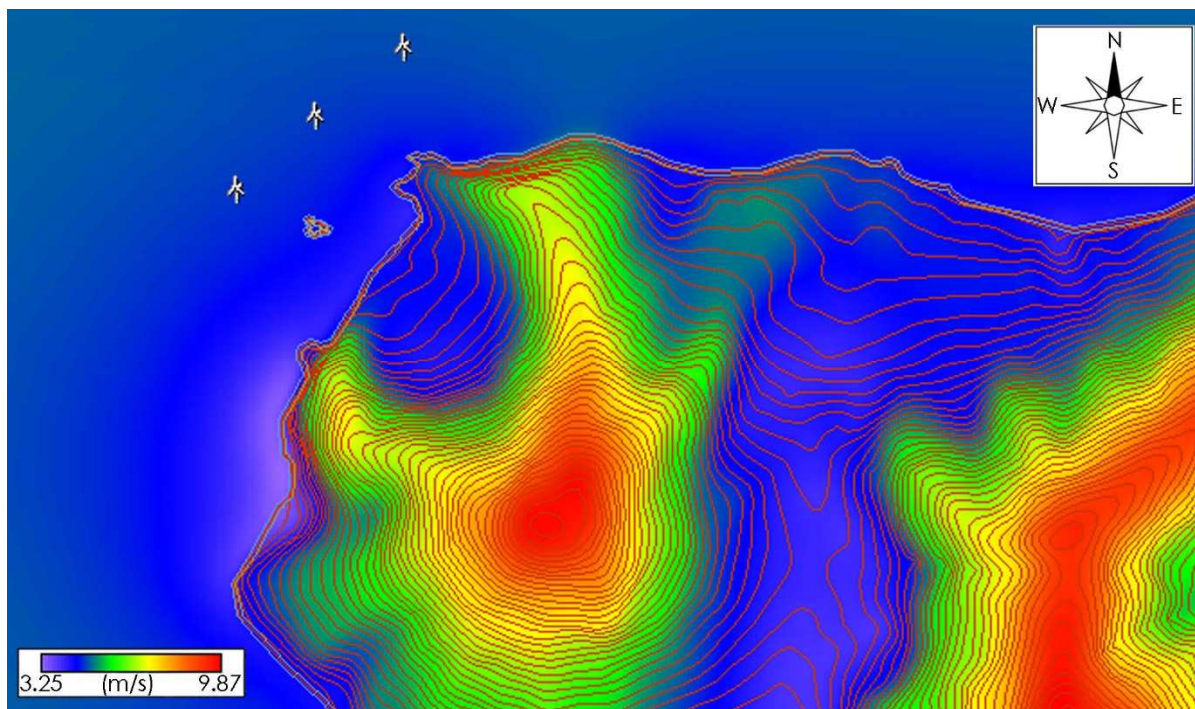


Figure 11: Wind potential map and siting of 3 wind turbines of 3 MW nominal power each at the western coast of Salina.

The wind roses at the wind turbines installation positions are shown in Figure 12.

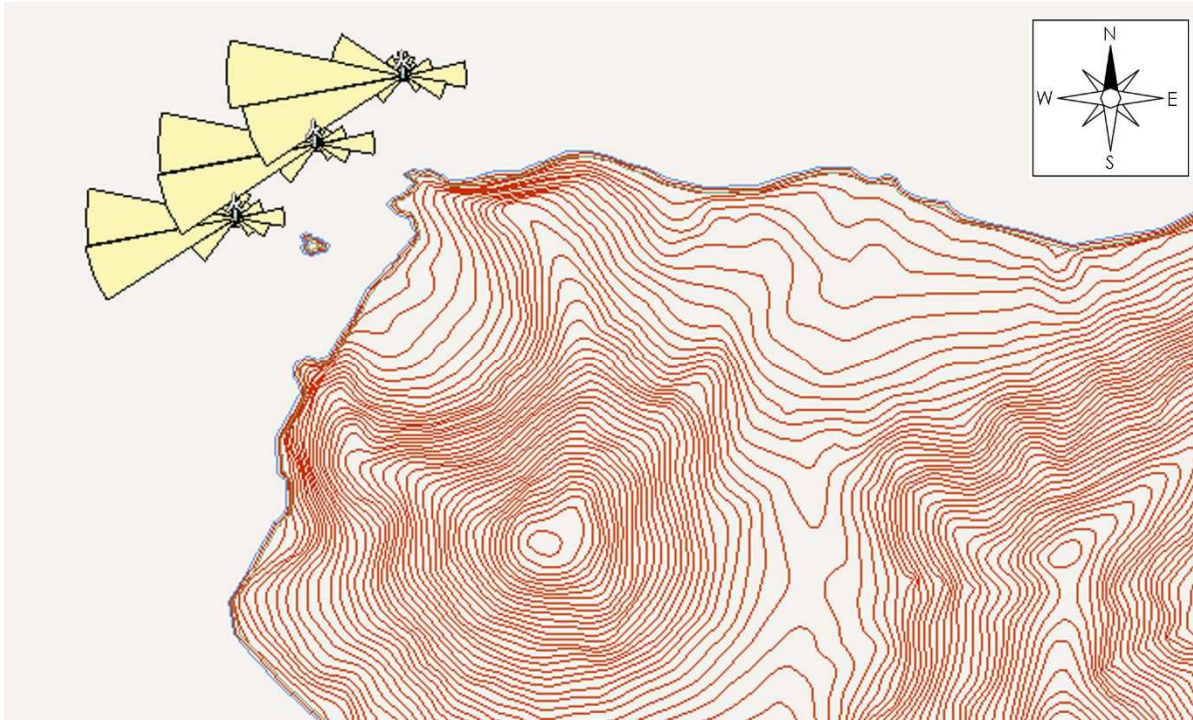


Figure 12: Wind-roses at the installation position of 3 wind turbines of 3 MW nominal power each at the western coast of Salina.

In Figures 13 the annual wind velocity wind roses and Weibull distributions are shown for the installation positions of the wind turbines and for the height of 100 m above sea level.

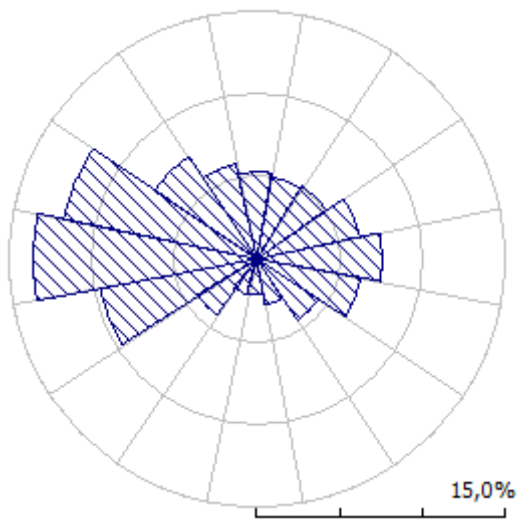


Figure 13a: Annual wind rose for the installation position of the first wind turbine 3MW.

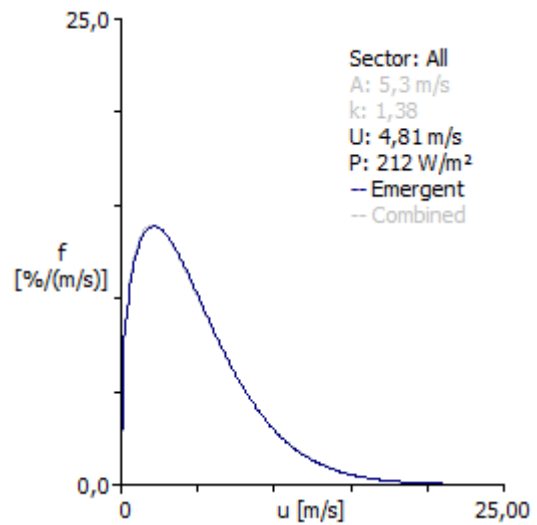


Figure 13b: Annual Weibull distribution for wind velocity the installation position of the first wind turbine 3MW.

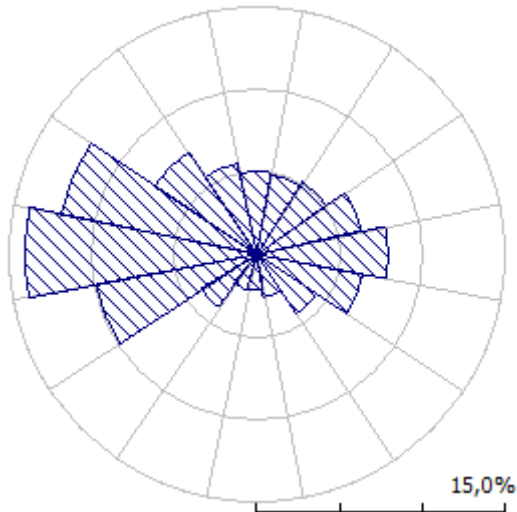


Figure 13c: Annual wind rose for the installation position of the second wind turbine 3MW.

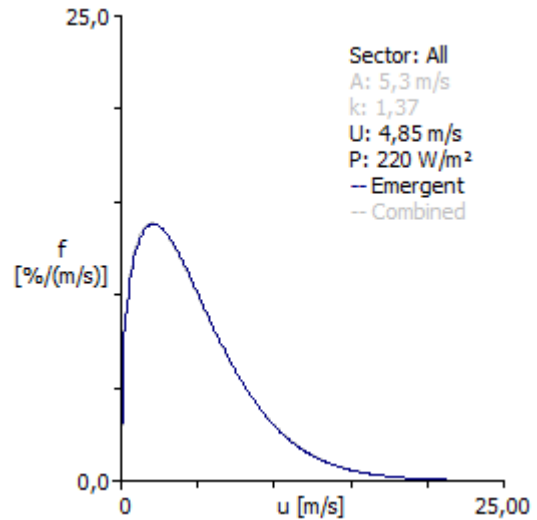


Figure 13d: Annual Weibull distribution for wind velocity the installation position of the second wind turbine 3MW.

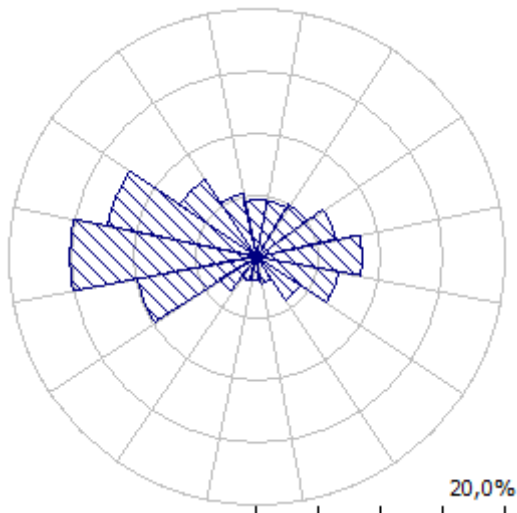


Figure 13e: Annual wind rose for the installation position of the third wind turbine 3MW.

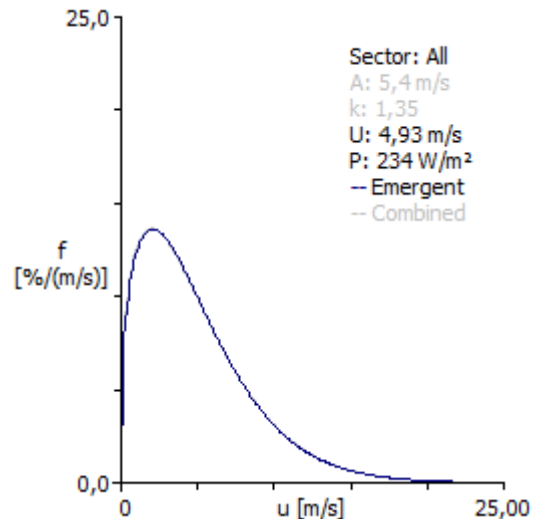


Figure 13f: Annual Weibull distribution for wind velocity the installation position of the third wind turbine 3MW.

The results regarding the siting positions and the annual electricity production from this dimensioning scenario are presented in Table 3.

Table 3: Annual electricity production analysis for the wind park with 3 wind turbines of 3 MW nominal power each.

Wind turbine	Installation position coordinates	Annual average wind velocity (m/s)	Annual average power density (W/m ²)	Net annual production (GWh)	Wake loss (%)	Capacity factor (%)
Wind turbine 1	38°34'50"N 14°47'46"E	4.81	212	5.252	1.09	19.98
Wind turbine 2	38°35'03"N 14°48'04"E	4.85	220	5.277	2.31	20.08
Wind turbine 3	38°35'14"N 14°48'22.39"E	4.93	235	5.501	1.81	20.94

Totals / average:	16.030	1.74	20.33
--------------------------	---------------	-------------	--------------

As seen in Table 3, the annual wake loss are kept below 2.5% with regard to the gross electricity production. Additionally, the low wind potential is clearly revealed by the calculated annual capacity factors.

Finally, a photorealistic representation of this first examined wind turbines siting is presented in Figure 14.

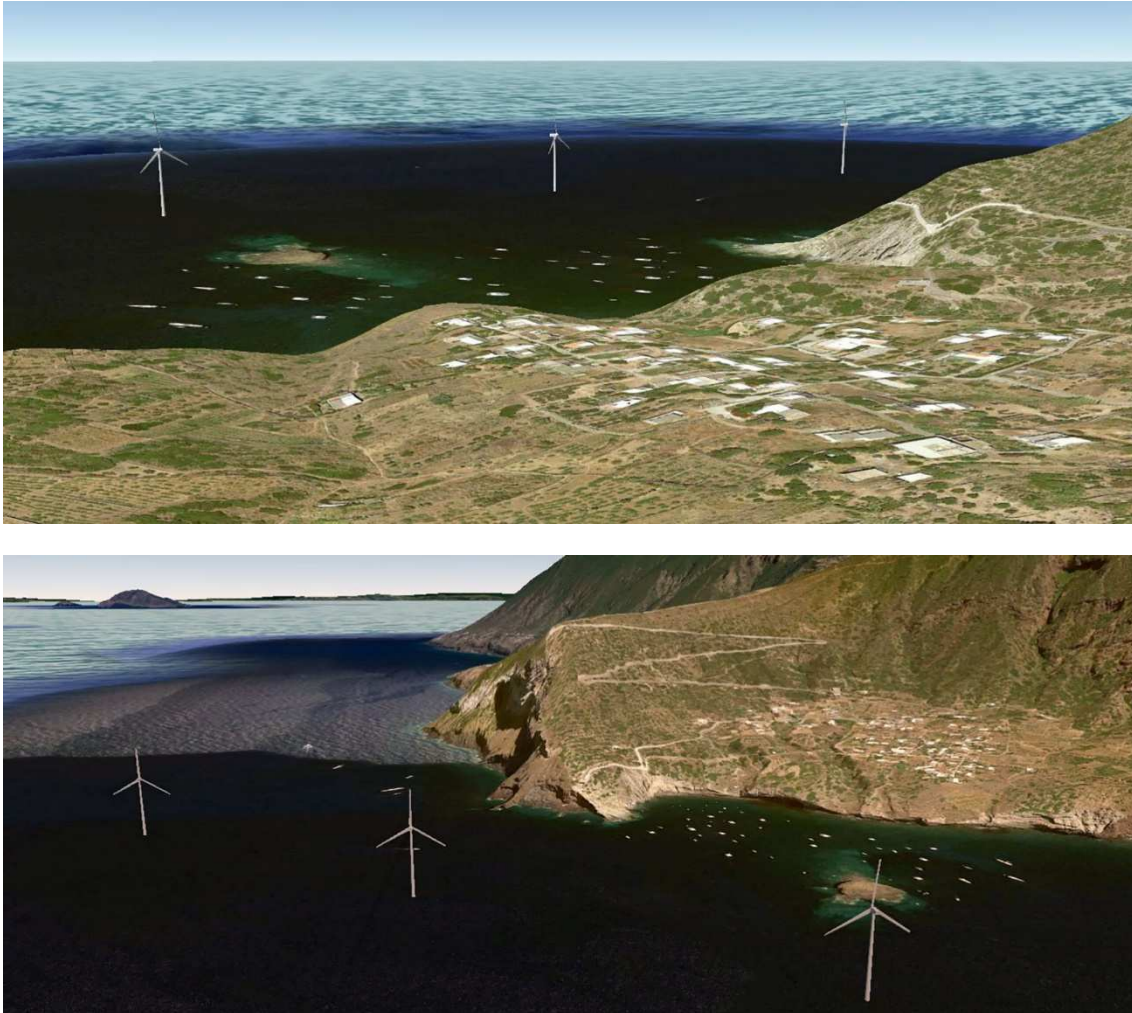


Figure 14: Photorealistic representation of the first examined offshore wind park.

Similarly, for the second investigated scenario, two wind turbines of 5 MW nominal power each were introduced. The siting of these wind turbines is presented in Figure 15, on an annual average wind velocity background, while in Figure 16, the wind rose at the wind turbines' installation positions are presented.

The results regarding the siting and the annual electricity production from this investigated scenario are shown in Table 4. As seen in Table 4, the larger wind turbine model with regard to the first investigated scenario has a negative impact on the total annual electricity production and the calculated capacity factors, which appear to be roughly 20% lower than in the first scenario. Nevertheless, in both cases the total electricity production from the offshore wind park is higher than the expecting future annual electricity consumption, with the transition of transportation and cooking needs from diesel oil and LPG to electricity.

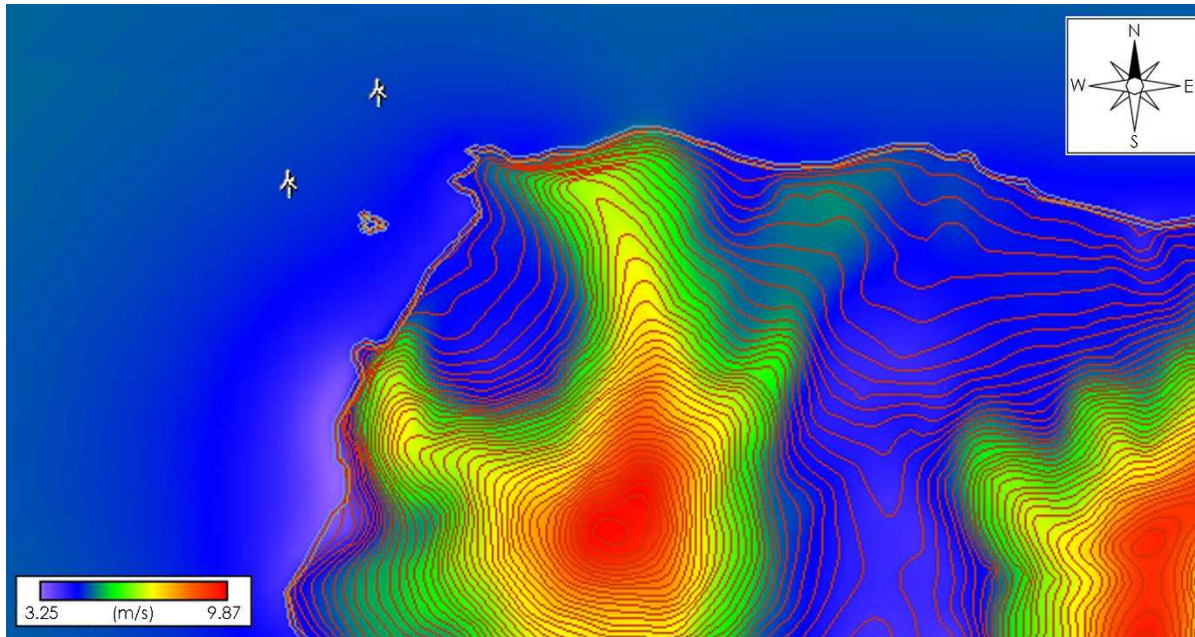


Figure 15: Wind potential map and siting of 2 wind turbines of 5MW nominal power each at the western coast of Salina.

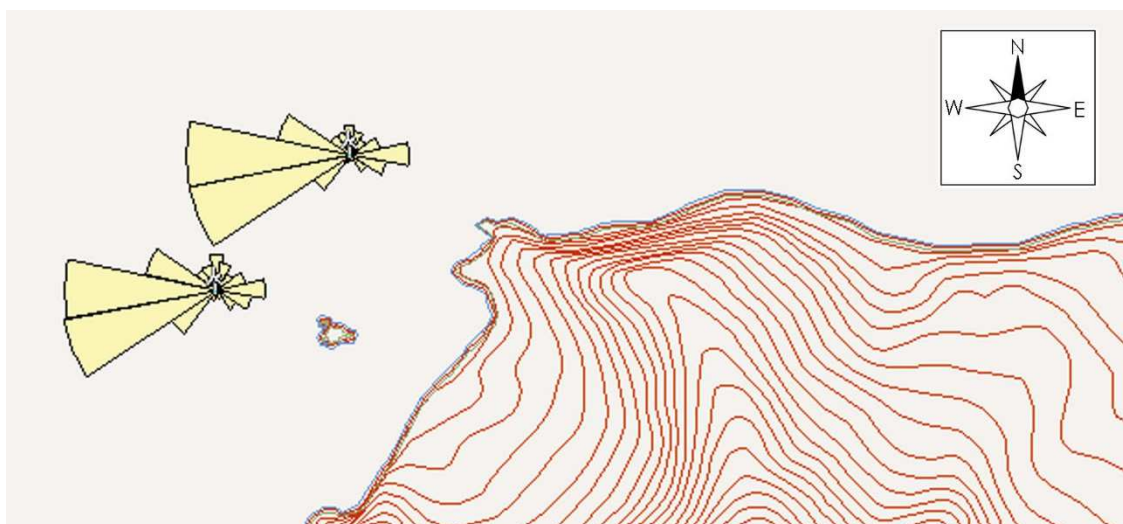


Figure 16: Wind-roses at the installation position of 2 wind turbines of 5MW nominal power each at the western coast of Salina.

Table 4: Annual electricity production analysis for the wind park with 2 wind turbines with 5 MW nominal power each.

Wind turbine	Installation position coordinates	Annual average wind velocity (m/s)	Annual average power density (W/m ²)	Net annual production (GWh)	Wake loss (%)	Capacity factor (%)
Wind turbine 1	38°34'51"N 14°47'46"E	4.86	222	7.051	1.31	16.10
Wind turbine 2	38°35'05"N 14°48'05"E	4.81	212	6.879	0.97	15.71
Totals / average:				13.930	1.14	15.90

The annual wind velocity wind roses and the Weibull distributions for the installation position of the wind turbines and the height of 100 m above sea level are shown in Figure 17.

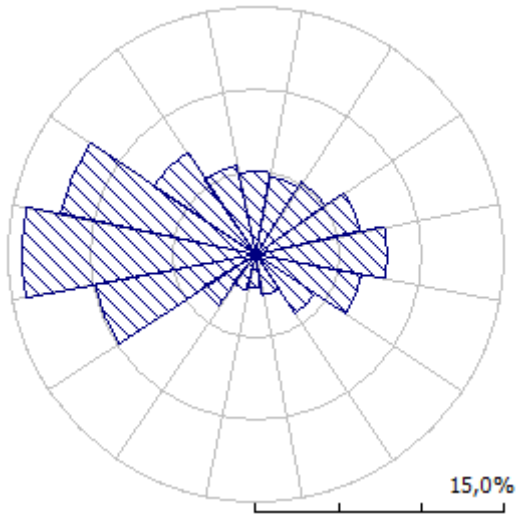


Figure 17a: Annual wind rose for the installation position of the first wind turbine 5MW.

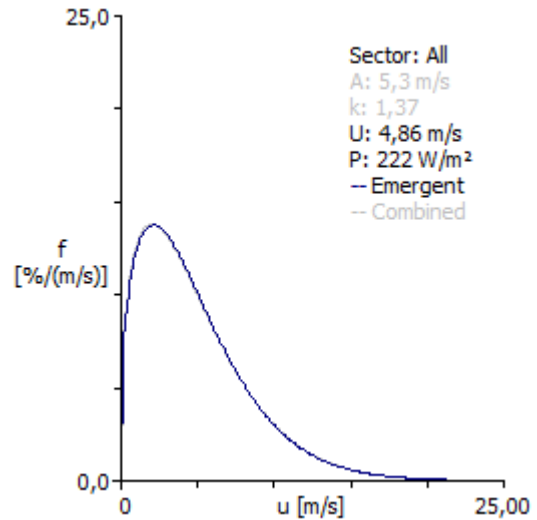


Figure 17b: Annual Weibull distribution for wind velocity the installation position of the first wind turbine 5MW.

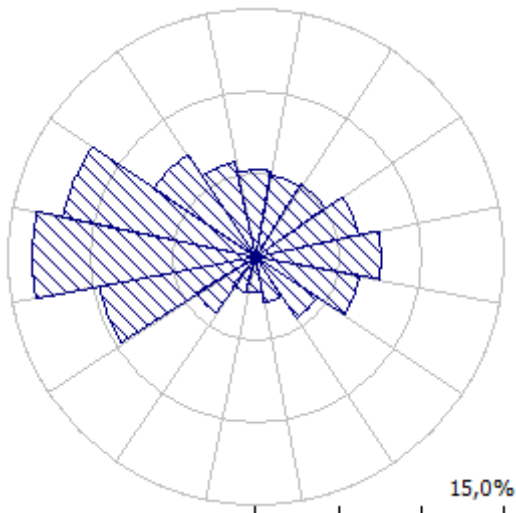


Figure 17c: Annual wind rose for the installation position of the second wind turbine 5MW.

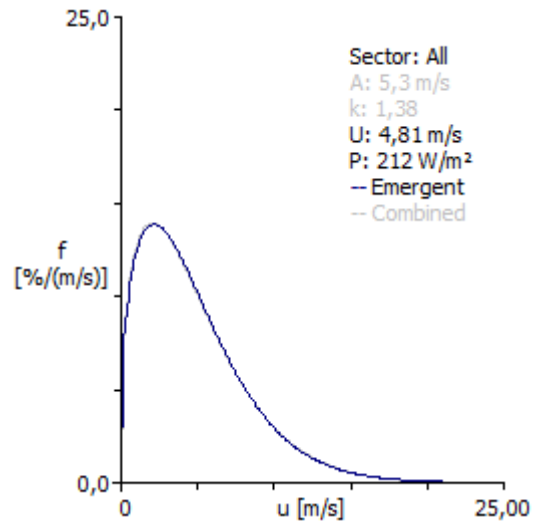


Figure 17d: Annual Weibull distribution for wind velocity the installation position of the second wind turbine 5MW.

Finally, photorealistic representations of this second examined wind turbines siting is presented in Figure 18.

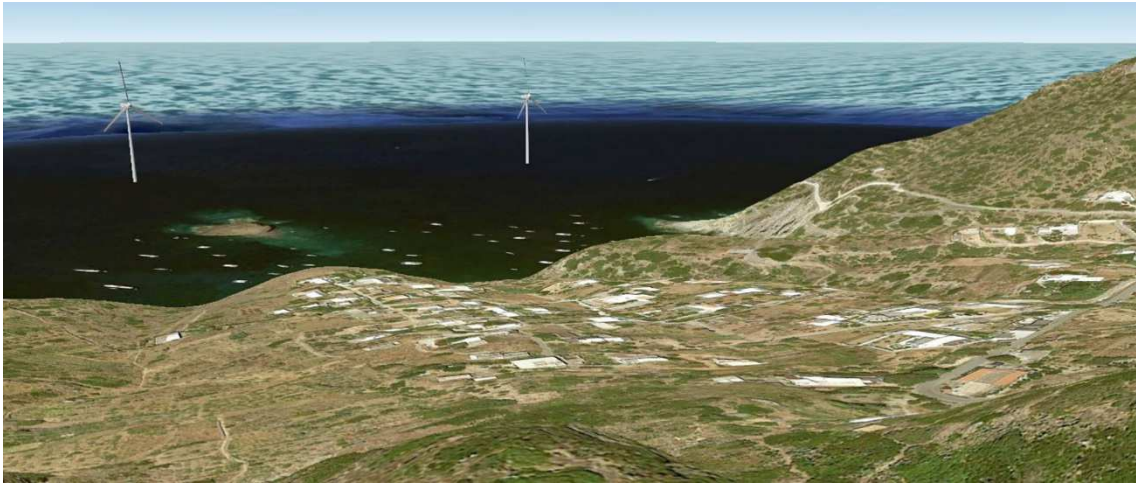


Figure 18: Photorealistic representations of the second examined offshore wind park.

3. Wave potential

Introduction

In general, energy is available and can be retrieved from the sea in three different ways: from the tidal currents, from the dynamic energy of waves and from the thermal gradients between the sea surface and depths close to 1 km, caused by temperature differences at the range of 25 °C. Ocean tidal, wave energy and thermal energy sources exhibit annual potentials of 800 TWh, 8,000–80,000 TWh and 10,000 – 80,000 TWh respectively, while the annual global electricity demand is configured at 16,000 TWh [5]. In this section, yet, given that this specific study refers to the island of Salina, we will focus particularly on the exploitation of the dynamic energy of surface waves, since no tidal currents are available in the specific island. Additionally, the Ocean Thermal Energy Converters (OTEC) employed for the exploitation of the sea thermal gradients have a specific power production of 30 – 80 kW/km² of sea surface [6]. This practically restricts the introduction of these systems in the open ocean sea and makes them inappropriate for the under consideration geographical area.

The exploitation of wave energy is a topic of research for more than two centuries. The first attempt to exploit wave potential is traced in France back in 1799 [7], while, since then, more than 1,000 patents have been created [8]. These patents exhibit a variety of different approaches, imposed by the alternative conditions and peculiarities met at each different location. The main parameters that can impact and inspire the configuration of a wave energy harvesting technology are the water depth and the distance from the coastline. Wave Energy Converters (WECs) can be installed on the coastline, close to the coastline or offshore. In general, the technologies located on or close to coastline exhibit easier accessibility, lower operation and maintenance cost, easier and less expensive electrical interconnection grid. On the other hand, normally, close to the coastline the available wave energy potential drops. Nevertheless, even this drawback is partially compensated due to wave refraction or diffraction from the coastline.

Since most people are not familiar with the concept and the distribution of wave potential globally, in this dedicated section a general approach is provided, starting from the theoretical and mathematical basis of wave energy, moving to an overall presentation of the wave potential distribution on global scale and ending at the presentation of the wave potential availability in the Mediterranean basin and to its estimation particularly at the under consideration geographical area. In this way, the readers will obtain an integrative picture of the concept of wave energy and they will also be able to compare the wave potential available at the under consideration area with regard to the globally wave energy resources.

Theoretical basis of wave energy

Particles of seawater surface moves towards the wind blowing direction as shown in Figure 19. Actually, a water particle located on the sea surface does not move towards a straight direction. It only executes a rotational movement returning always at the same point on sea surface. The diameter of this rotational movement defines the significant wave height, designated as H in this figure. The time required for a full rotational movement of a water particle defines the significant wave period T . The significant wave period represents the period of a sinusoidal wave with the same energy content as the sea wave. The distance between two consecutive wave crests on sea surface defines the wave's length, designated as L in Figure 19. Finally, another significant parameter that affects the wave energy is the

uninterrupted distance on sea surface over which the wind blows without any physical (e.g. an islands or an isle) or technical obstacle that may cause a significant effect on the wind velocity magnitude or direction. This distance is known as “fetch”.

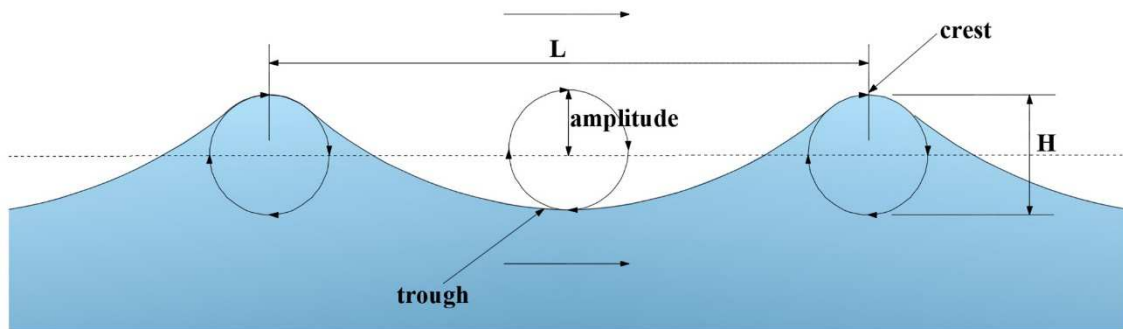


Figure 19: Fundamental wave motion and characteristic features and magnitudes.

The significant wave height H can be related with the blowing wind velocity u with the following relationship introduced by Scripps [9]:

$$H=0.085 \cdot u^2 \quad (4)$$

The wave's length L is given by the following relationship as a function of the wave period T and the speed of the wave c , known as “celerity”:

$$L=c \cdot T \quad (5)$$

Typical values for the above mentioned characteristic wave features are presented in Table 5 [10].

Table 5: Conditions necessary for a fully developed sea at given wind speeds, and the parameters of the resulting waves.

Wind conditions				Wave size			
Wind speed in one direction (km/h)	Wind force (Beaufort)	Fetch (km)	Wind duration (h)	Average wave height (m)	Average wave length (m)	Average period (s)	Average wave celerity (km/h)
19	3 - 4	19	2	0.27	8.5	3.0	10.2
37	5 - 6	139	10	1.5	33.8	5.7	21.4
56	7	518	23	4.1	76.5	8.6	32.0
74	8 - 9	1,313	42	8.5	136.0	11.4	42.9
92	10	2,627	69	14.8	212.2	14.3	53.4

The total mechanical energy density E_m of waves (in J/m^2 of sea surface) changes continuously between kinetic energy (exclusive form of energy at the waves' troughs) and potential energy (exclusive form of energy at the waves' crests). At any time moment, the total mechanical energy of waves is given by the following relationship [11]:

$$E_m=E_{k-tr}=E_{p-cr}=\rho \cdot g \cdot \frac{H^2}{16} \quad (6)$$

where ρ is the seawater density (roughly equal to $1,025 \text{ kg/m}^3$) and g is the acceleration of gravity (9.81 m/s^2).

As seen in the above relationship, the overall mechanical energy density is transformed exclusively to kinetic energy density at the waves' troughs E_{k-tr} and exclusively to potential energy density at the waves' crest E_{p-cr} . In the above relationship, E_m , E_{k-tr} , E_{p-cr} are in J/m^2 .

The water power intensity (in kW/m of wave crest) is given by the following relationship:

$$P = \frac{\rho \cdot g^2}{64 \cdot \pi} \cdot H^2 \cdot T \quad (7)$$

The above relationship stands for deep water conditions, defined as the cases with sea depth d_s higher than the half of the wave length L : $d_s > 0.5 \cdot L$.

According to the indicative features presented in Table 5, with a wind velocity of 74 km/h and a fetch of roughly 1,300 km, the expecting waves of 8,5 m height and 11.4 s period will have a power density of:

$$P = \frac{\rho \cdot g^2}{64 \cdot \pi} \cdot H^2 \cdot T \Rightarrow P = \frac{1,025 \cdot 9,81^2}{64 \cdot \pi} \cdot 8,5^2 \cdot 11,4 \Leftrightarrow P = 404,1 \text{ kW/m}$$

Finally, the water power density is also given as a function of the waves' mechanical energy density E_m and the waves' celerity c by the following relationship:

$$P = E_m \cdot c \quad (8)$$

The global wave potential

Figure 20 shows a general view of the available wave potential on earth [12] in terms of the annual average wave power density (in kW/m).

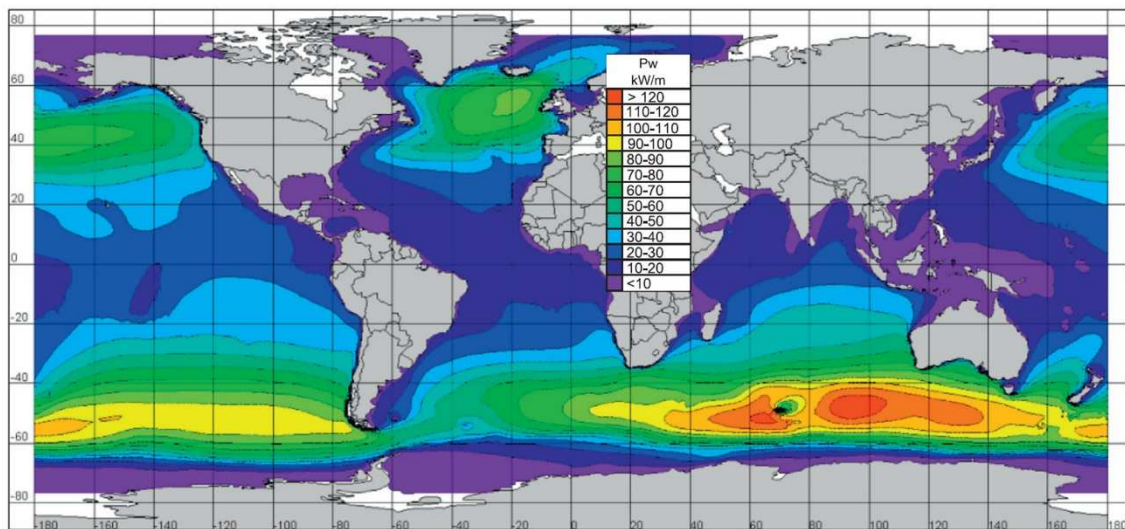


Figure 20: Global distribution of annual average wave power density (in kW/m) based on 10-year measurements [12].

As seen in this figure, the highest wave potential is found between the geographical latitudes of 40° and 60° , both in North and South Hemisphere. Particularly in South Hemisphere, the wave potential is found higher than in the North, because of the larger areas of open sea, without any pieces of land at all. Indicatively, in the ocean seas at the south of Australia, New Zealand and South America, there are extensive areas found with wave power density higher than 120 kW/m. On the other hand, in the North Hemisphere the highest wave potential is found between 80 kW/m and 90 kW/m at the west coast of Great Britain and at the south of Iceland.

The highest wave potential close to shore in the North Hemisphere is also found at the above mentioned locations. This is better depicted in Figure 21, which presents the distribution of the available wave potential in Europe [13], again in terms of the annual average wave power density. High wave potential, at the range of 60 kW/m is also found in the Pacific Ocean, at the west coast of Canada and U.S.A.

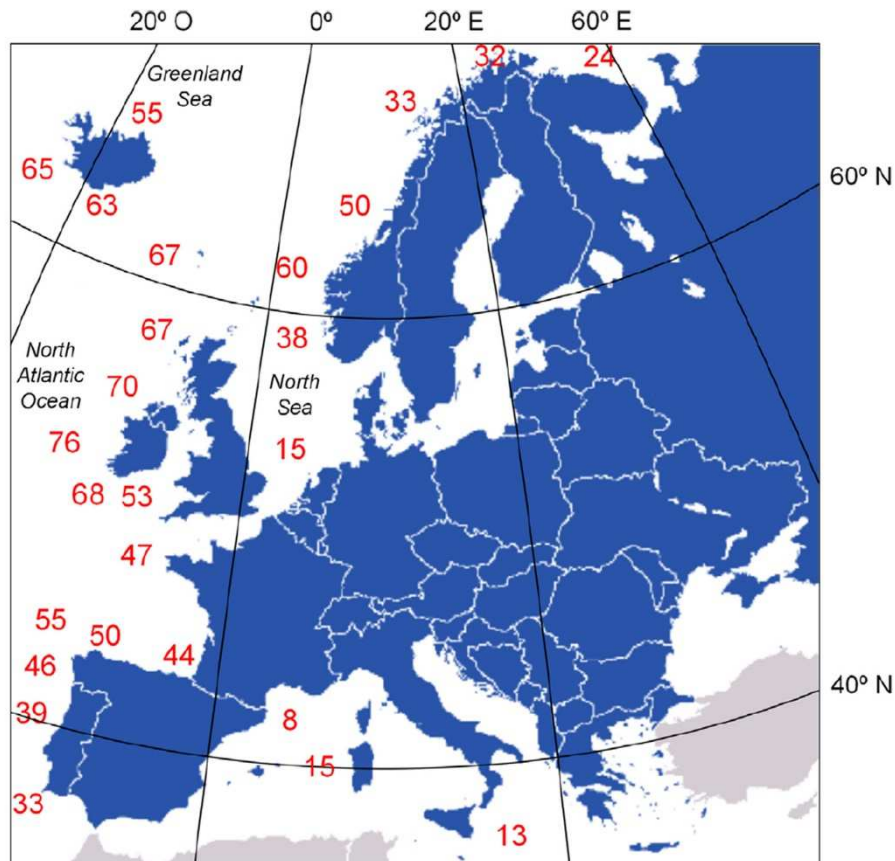


Figure 21: Typical annual average wave power density for several locations in Europe [13].

Apart from the magnitude of the wave energy potential, another crucial factor is its variability. Obviously, as with any other fluctuating renewable energy source (e.g. wind, solar radiation), the available wave potential is desirable to be as steady as possible. This is imposed by:

- the requirement to avoid long periods of wave potential lower than the wave energy converters operation range, which would lead to reduced electricity production
- the necessity to avoid extremely high wave potential, which, while being unexploited, it will also introduce serious risk for the safety of the wave energy converters.

The temporal variability of the wave potential is expressed by an index introduced for this specific purpose, called Coefficient of Variation (CoV), defined as the ratio of the standard deviation σ of the wave power density time series $P(t)$ over the average value μ of the same time series [14]. It is given by the following relationship:

$$\text{CoV} = \frac{\sigma(P(t))}{\mu(P(t))} \quad (9)$$

Obviously, the bigger the CoV for a specific geographical region, the higher the wave energy potential variability. CoV equal to 0 implies absence of variability. CoV equal to 1 means that the standard deviation of the captured time series equals to its average value. Figure 22 presents the global fluctuation of the CoV ratio based on 10-year measurements of the wave

power density [12]. As seen in this figure, it seems that the close to the poles ice-covered geographical regions exhibit the highest variability of the wave potential, both on the South and the North Hemisphere, with CoV values higher than 2.8. The highly interesting regions with the highest wave potential between latitudes of 40° and 60° in the Pacific and the Atlantic Ocean exhibit moderate CoV values at the range of 1.4 – 1.8. The lowest CoV values are found in the equator zone.

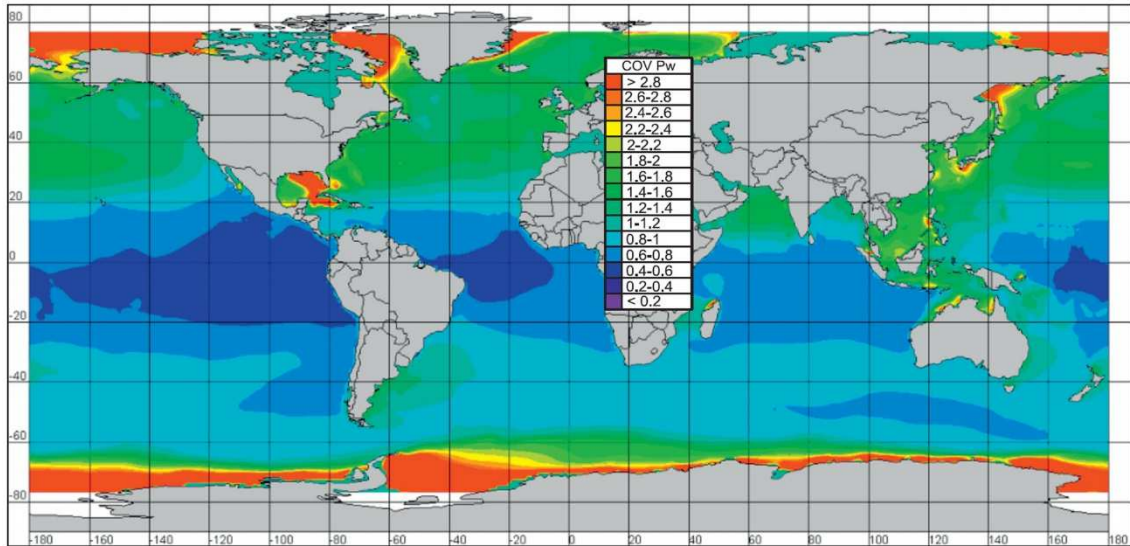


Figure 22: Global fluctuation of the ratio CoV based on 10-year measurements of the wave power density [13].

Finally, in Table 6 the total globally calculated theoretical wave power is presented, firstly as the overall gross wave power P_{gross} , secondly the available wave power P excluding all regions with wave potential lower than or equal to 5 kW/m and finally the net power wave P_{net} , corresponding to all not ice-covered areas with wave power higher than 5 kW/m [15].

Table 6: Global distribution of the available theoretical wave potential.

Location	P_{gross} (GW)	P (GW)	P_{net} (GW)
Europe (N and W)	381	371	286
Baltic Sea	15	4	1
European Russia	37	22	3
Mediterranean	75	37	37
North Atlantic Archipelagos	111	111	111
North America (E)	115	103	35
North America (W)	273	265	207
Greenland	109	99	3
Central America	180	171	171
South America (E)	206	203	202
South America (W)	325	324	324
North Africa	40	40	40
West and Middle Africa	77	77	77
Africa (S)	178	178	178
Africa (E)	133	133	127
Asia (E)	173	164	157

Table 6: Global distribution of the available theoretical wave potential.

Location	P _{gross} (GW)	P (GW)	P _{net} (GW)
Asia (SE) and Melanesia	356	283	283
Asia (W and S)	100	90	84
Asiatic Russia	172	162	23
Australia and New Zealand	590	574	574
Polynesia	63	63	63
Total	3,709	3,474	2,986

Looking at Table 6, we may conclude that Europe has one of the highest contributions on the global wave potential share. Specifically, regarding the net power wave power, only the ocean sea at the south of South America and Australia exhibits higher values than the one in Europe. On the other hand, by looking at Figure 21, we may observe the high spatial variability of the wave potential in the European seas. As expected, the highest values are met in the western coastline of the United Kingdom and Norway, as well as of Iceland, with annual average wave density that can exceed 70 kW/m. Quite high potential is also available at the Atlantic shore of the Iberian Peninsula, reaching annual average wave power density higher than 50 kW/m, while in the close Baltic or Adriatic sea the annual average wave power density varies at 2 – 3 kW/m.

In the Mediterranean Sea, which is the under consideration geographical area for the specific study, the higher wave power density is found at the western regions, between the Balearic Island and Sardinia, while it becomes considerably lower at the eastern part of the Sea. More on the available wave potential in the Mediterranean Sea and particularly for the Italian coast and the island of Salina are given in the next section.

Wave potential in Mediterranean Sea

The wave potential in the Mediterranean Sea exhibits high spatial variability, due to the intensive alternations between land and sea, which can be summarized in the closed basins found mainly in the eastern part of the Sea (e.g. Adriatic Sea, Aegean Sea) and the relatively open sea in the western part of the Sea, between the Balearic Islands and the islands of Corsica and Sardinia, as well as in the middle and south Mediterranean, between Malta and Crete. This mosaic of sea, mainland and insular territories formulate the wave potential distribution depicted in Figure 23 [16].

This wave potential map has been developed with computational models, based on meteorological and wave data measurements from the period 2001 to 2010. As seen in Figure 23, the Mediterranean Sea could be divided in the following regions, with regard to the available wave potential:

- The area between the Balearic Islands and Corsica and Sardinia, as well as the western coast of Sicily, which is the richest area regarding wave potential, with annual average wave power density from 10 kW/m to 15 kW/m. This part of the Mediterranean Sea can be considered that they belong to an intermediate level regarding wave potential, compared to the higher value of the western European Atlantic coast.
- The middle and south Mediterranean Sea, between Malta and Crete, with annual average wave power density at 7 kW/m to 9 kW/m.
- The eastern part of the Mediterranean basin, between Crete and Cyprus, with slightly reduced wave potential, between 6 kW/m and 7 kW/m.

- Finally, all the closed basins, like the Adriatic Sea, the northern part of the Tyrrhenian Sea and the Aegean Sea (with the exception of its north-east part), which have sensibly reduced wave potential, with annual average wave power density lower than 3 kW/m.

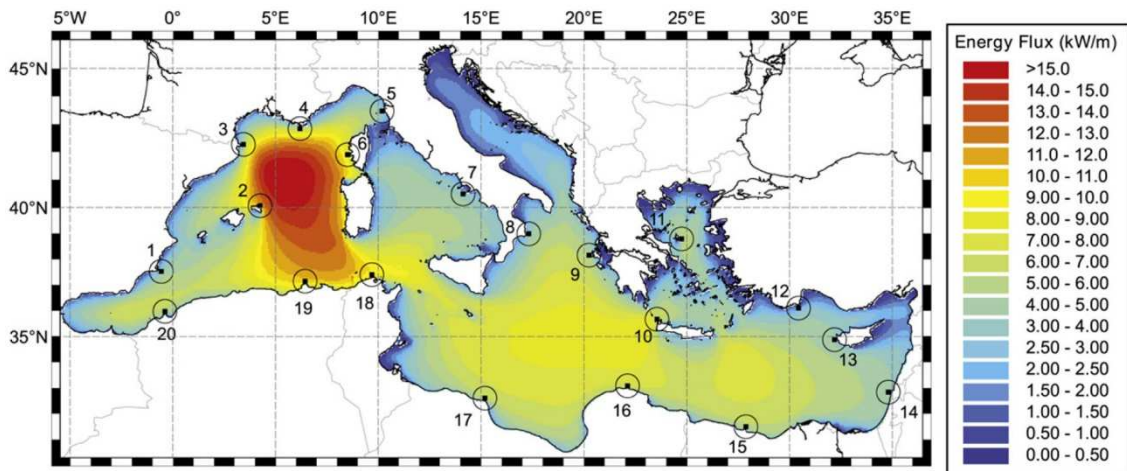


Figure 23: Spatial variation of the annual average wave power density in the Mediterranean Sea [16].

In Table 7 the wave potential availability is provided in the form of the annual average power density (in kW/m) and the annual average energy density (in MWh/m), for 20 specific coastal regions, shown also in Figure 23 [16].

No	Site	Depth (m)	Annual average power density (kW/m)	Annual average energy density (MWh/m)
1	Cabo de Palos (Es)	121	3.91	34.25
2	Menorca (Es)	65	10.90	95.48
3	Cabo Creus (Es)	439	5.34	46.78
4	Hyères (Fr)	1,476	6.47	56.68
5	Livorno (It)	83	3.24	26.02
6	Ajaccio (Fr)	786	8.44	73.93
7	Napoli (It)	782	3.51	30.70
8	Crotone (It)	615	3.70	32.41
9	Kefallonia (Gr)	1,512	4.91	43.01
10	Ag. Gramvousa (Gr)	374	7.10	62.20
11	Skyros (Gr)	269	5.16	45.20
12	Gelydonia Burnu (Tr)	444	2.26	19.80
13	Peyia (Cy)	1,290	3.83	33.55
14	Haifa (Il)	252	4.02	35.22
15	Ras El-Kanayis (Eg)	420	5.30	46.43
16	Ras Al Hilal (Ly)	374	6.59	57.73
17	Misrata (Ly)	161	5.68	49.76
18	Ras Angela (Tn)	250	9.25	81.03
19	Cap Bougaouni (Dz)	2,354	10.33	90.49
20	Orano (Dz)	1,428	5.15	45.11

The annual average wave power density only provides a rough estimation on the available wave potential in an area and a general index regarding whether it is worthy or not to proceed to further investigation on the development of wave energy projects in the area. Beyond the annual average available wave power density in the Mediterranean basin, considerably important is its temporal variability. Aiming to provide a deeper insight on the available wave potential in the Mediterranean Sea, average seasonal wave potential maps are developed for each different season of the year (winter, spring, summer, autumn). These maps are presented in Figure 24.

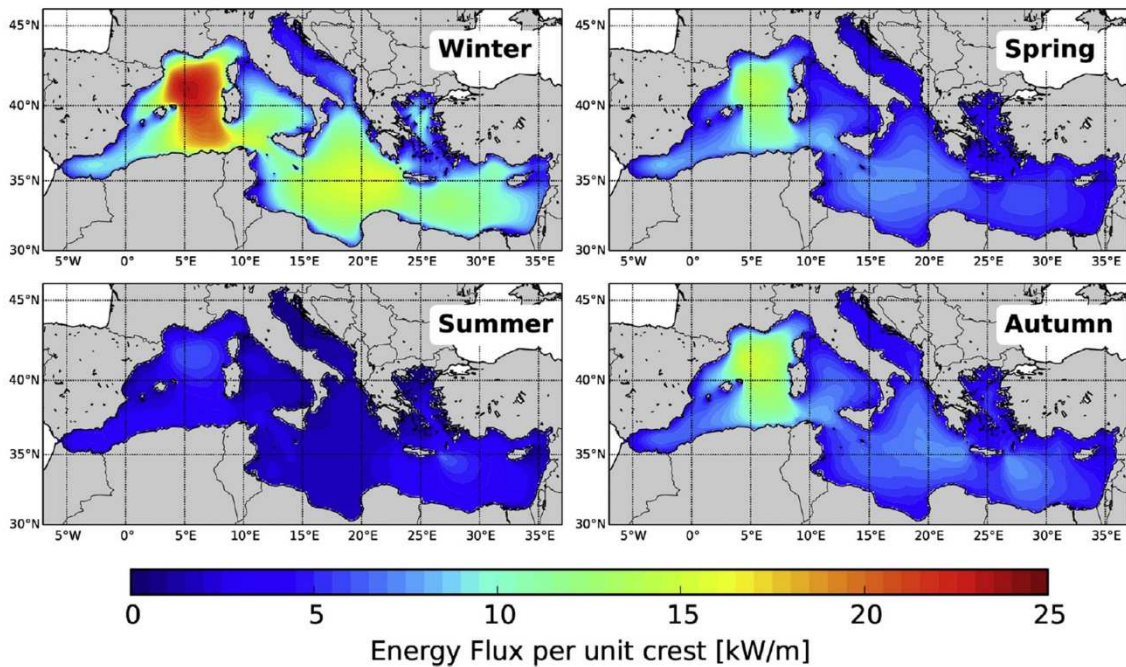


Figure 24: Spatial variation of the seasonal average wave power density in the Mediterranean Sea [17].

As seen in Figure 24, there is significant seasonal variability on the available wave potential in Mediterranean Sea. The higher wave potential is observed during winter, obviously due to the prevailing weather conditions. During this period, the average wave power density reaches values higher than 20 kW/m (between the Balearic Islands and Corsica and Sardinia), while at the west of Crete, the seasonal average wave potential exceeds 15 kW/m. Autumn and spring have the same wave potential pattern with winter, yet with considerably reduced average wave power density, which can reach values at 15 kW/m, again between Balearic Island and Corsica. Autumn seems to have slightly higher wave potential than spring. Finally, in summer, the wave potential appears significantly reduced for the whole basin. The pattern maintained during the rest annual period (from autumn to spring) is lost. There is only one area that seems to have slightly higher wave potential (at the range of 6 kW/m to 8 kW/m) at the eastern coast of Crete. In all other regions, the seasonal average wave power density remains lower than 6 kW/m.

Finally, in Figure 25, the spatial variability of CoV for the Mediterranean Sea is presented. As seen in this Figure, the temporal variability of the wave potential in the Mediterranean Sea is much lower than in global scale (see Figure 20). The highest values on annual basis are mainly found in areas with low wave potential, e.g. the Alboran Sea, the North Aegean Sea, the Eastern Tyrrhenian Sea and the Gulf of Sidra (north cost of Libya). In these cases, the annual CoV is calculated maximum at 0.20. For the areas with the highest wave potential, the CoV is calculated lower than 0.15 (west of Sardinia) or even lower than 0.13 (west of Crete). The

above figures indicate a relatively reduced annual variability of the wave potential, which certainly favours the development of wave energy projects in the area. What is also more important, is that, given the seasonal wave potential maps presented in Figure 24, this annual variability is mainly due to the reduced wave potential during the summer period and not due to extremely high wave potential during winter, formulated by adverse weather conditions, which, on the one hand wouldn't be exploitable and, on the other, would impose serious safety risk for the wave energy converters.

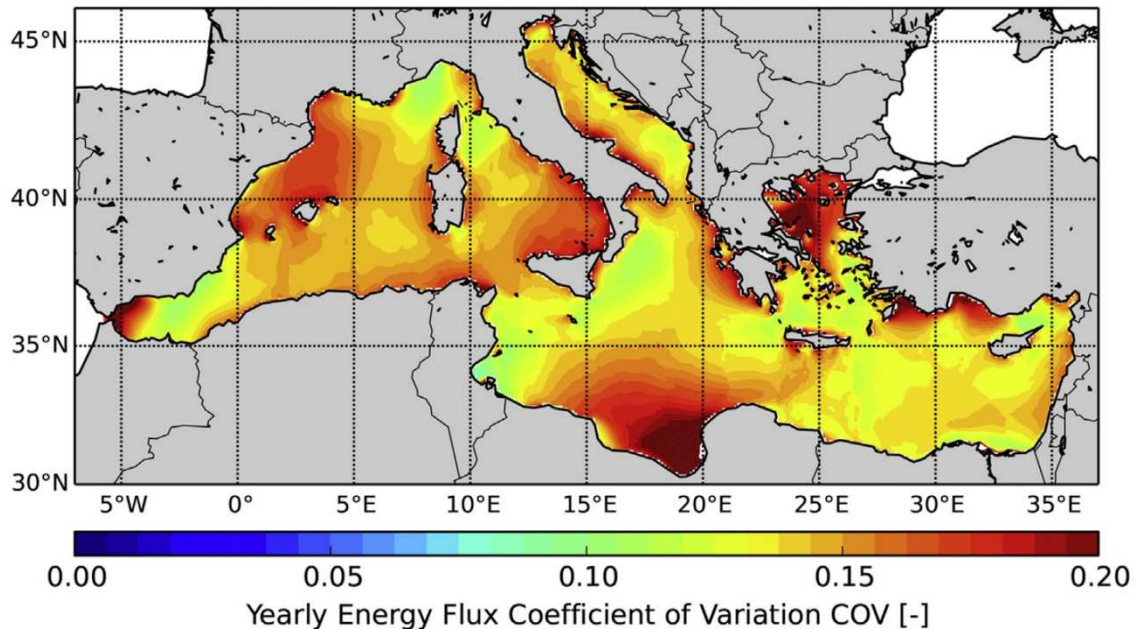


Figure 25: Spatial variation of the CoV on annual basis in the Mediterranean Sea [17].

Wave potential in the Italian coast and in the Salina Island

The western Italian coast has some areas with the highest wave potential in the Mediterranean. First of all, as already stated in the previous section, the western coast of Sardinia and the open sea at the west part of the island exhibits the highest annual average wave power density in the Sea, with values higher than 15 kW/m. Another interesting case is the sea area at the west and the western of Sicily, with annual average wave power density around 9 – 10 kW/m.

A closer look of the wave potential at the western coast of Sardinia and the west, north-west and south coast of Sicily is given in Figure 26a and 26b respectively [16] for a line parallel to the coastline at a distance of 12 km from the latter. The depth in this distance is always higher than 50 m and any effect of the bathymetry on the wave potential should be negligible. As seen in Figure 26a, the highest wave potential at the western coast of Sardinia is found at the northern and southern coast, north of Alghero and at the region of San Pietro Island. The annual average wave power density in these areas is estimated at 10 – 12 kW/m. Regarding Sicily, the most interesting coastal part seems to be the western part of the island, at the area of Favignana Islands, where the annual average wave power density is calculated at 7 – 8 kW/m. Moving from the western cape of Sicily to northwest and finally to the west, the wave potential gradually reduces and drops eventually below 3 kW/m at the north coast, west of Palermo.

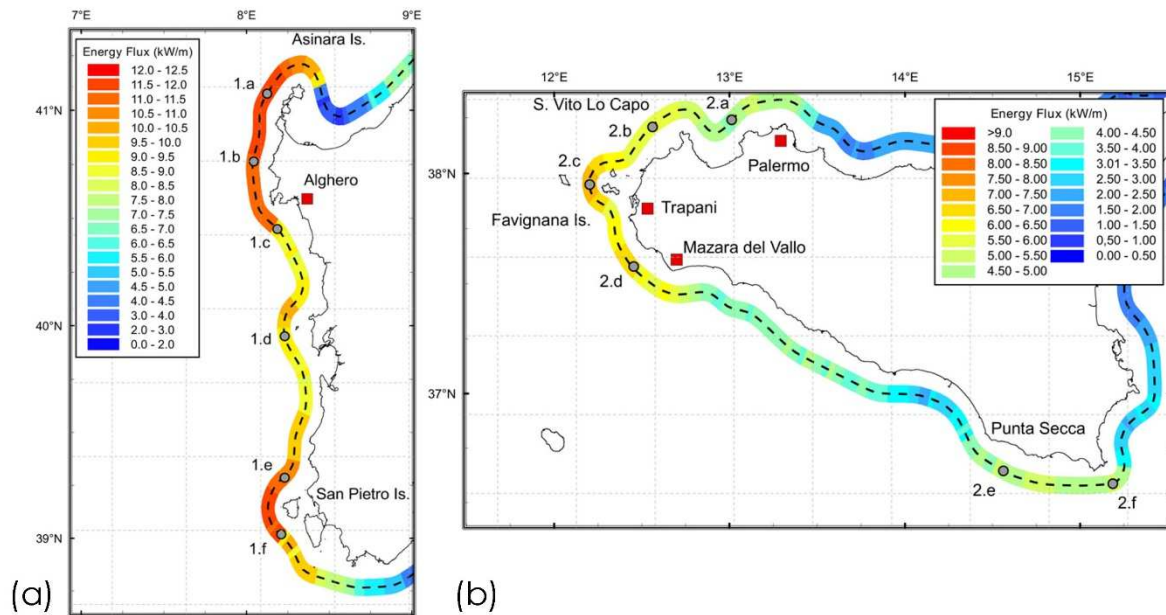


Figure 26: The wave potential at the coasts of Sardinia and Sicily [16].

Regarding the available wave potential particularly in the under interest area, there were no literature data found in any published article or report. However data are available from the ERA – Interim database of the European Centre for Medium-Range Weather Forecasts (ECMWF), for the period 1979 – 2018 [18, 19]. Specifically, meteorological data are available for 6-hour intervals and for the following required magnitudes:

- mean wave direction
- mean wave period
- significant height of combined wind waves and swell.

The above data were retrieved for the period from 1979 to 2014 and for the closest measurement point at the under interest area ($38^{\circ} 45' N$, $14^{\circ} 45' E$). The location of this measurement point is shown in Figure 27 with regard to the location of the Salina Island. The distance from the northwest cape of the Island is calculated at 19.9 km.

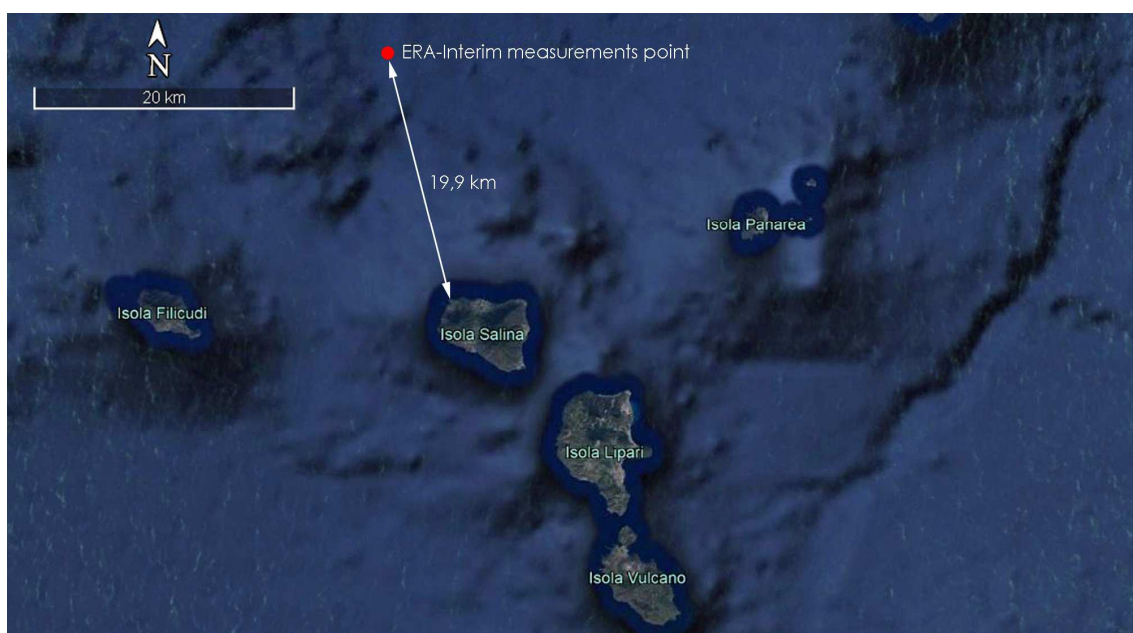


Figure 27: Location of the ERA-Interim measurement point with regard to the Salina Island.

Given the retrieved wave potential data, in Figure 28 the annual average wave power density is plotted from 1979 to 2014. In this figure it is seen that there are years with the annual average wave power density lower than 3 kW/m of wave length, while, during the examined 36-year time period, for only two years (in 1981 and in 2010) this feature was higher than 5 kW/m. These indications reveal the relatively low wave potential available in the under interest area.

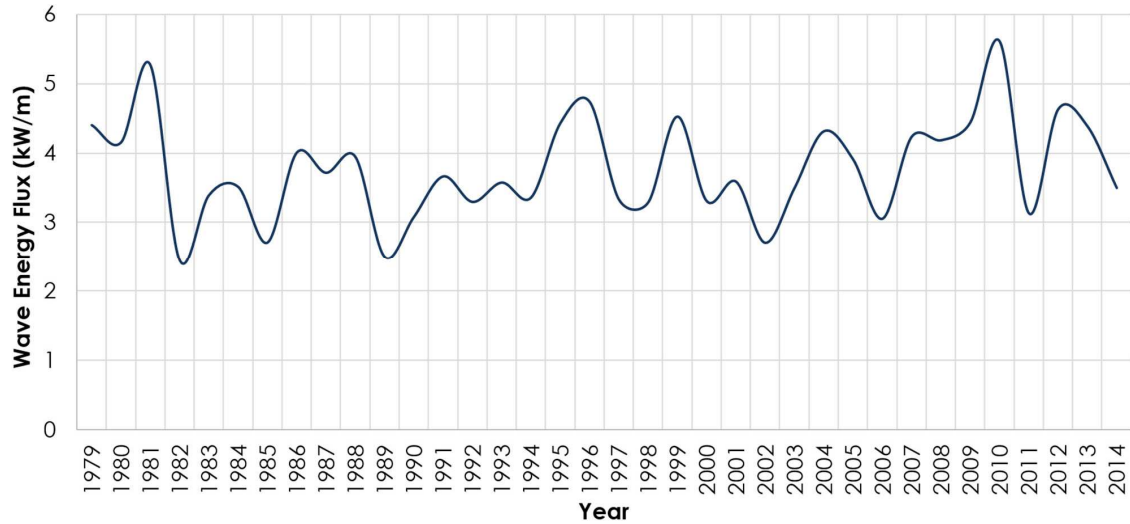


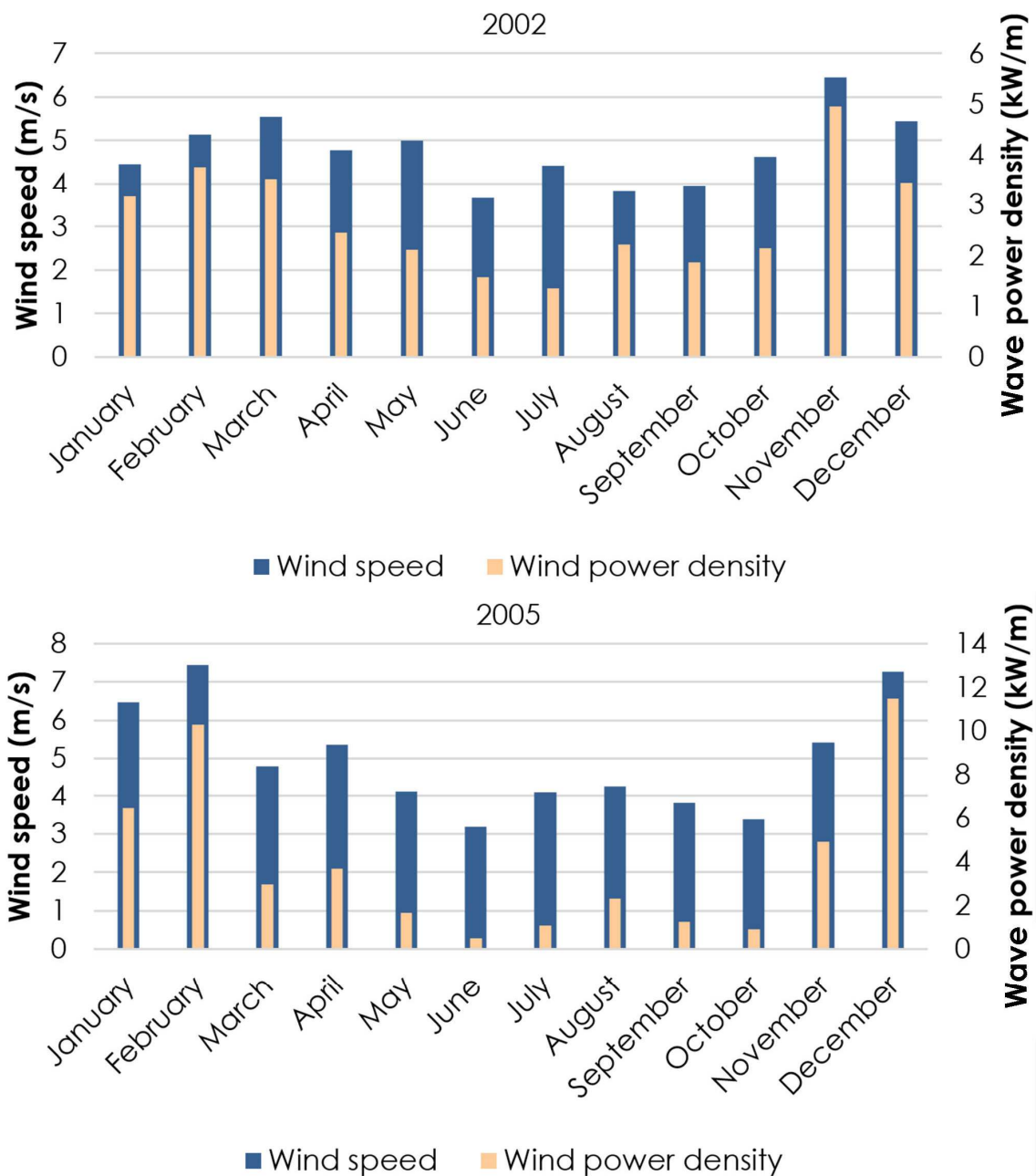
Figure 28: Fluctuation versus time of the annual average wave energy flux at the under consideration area [18, 19].

A more detailed insight in the available wave potential at the specific geographical point is given in Table 8. In this table, the monthly average values for the wind speed and the wave power density is presented at the above mentioned measurement point for three indicative years, one of low annual average wave power density (2002, 2.7 kW/m), one of medium (2005, 3.9 kW/m) and one of high (2010, 5.7 kW/m).

Table 8: Monthly analysis of the available wave potential measurements for three indicative years.

Month	2002		2005		2010	
	Wind speed (m/s)	Wave power density (kW/m)	Wind speed (m/s)	Wave power density (kW/m)	Wind speed (m/s)	Wave power density (kW/m)
January	4,455	3,166	6,462	6,434	7,424	14,928
February	5,135	3,758	7,453	10,290	7,844	11,944
March	5,538	3,523	4,791	2,941	5,535	5,384
April	4,783	2,450	5,353	3,661	4,033	1,508
May	4,993	2,111	4,105	1,650	5,251	5,287
June	3,655	1,580	3,184	0,475	4,510	2,458
July	4,421	1,356	4,093	1,068	3,416	0,926
August	3,817	2,219	4,265	2,311	3,890	0,929
September	3,948	1,869	3,823	1,248	3,903	2,414
October	4,616	2,150	3,392	0,914	4,950	2,954
November	6,455	4,958	5,412	4,900	6,829	11,034
December	5,442	3,447	7,274	11,496	6,442	8,152
Annual average	4,771	2,716	4,967	3,949	5,336	5,660

The results of Table 8 are also summarized graphically in Figure 29. From Table 8 and Figure 29, it is seen that the wave potential is mainly configured by the available wind potential during winter. This is clear by comparing the first graph referring to 2002 (low annual wave potential) to the corresponding graphs referring to 2005 and 2010 (medium and high annual wave potential). It is obvious that the low wind speeds captured in winter period in 2002 (from 4.4 m/s to 5.4 m/s) contributed to the configuration of respectively low wave potential during the same season, which, in turn, affected the total annual average wave potential of the whole year. It is worthy of mentioning that the average wave power density in July and in August in 2002 is higher than the same figures for 2010, which exhibits the highest annual average annual wave power density for all the three investigated years. Nevertheless, this does not affect the overall annual content of 2002 or 2010, which is obviously imposed by the availability of wave potential particularly during winter.



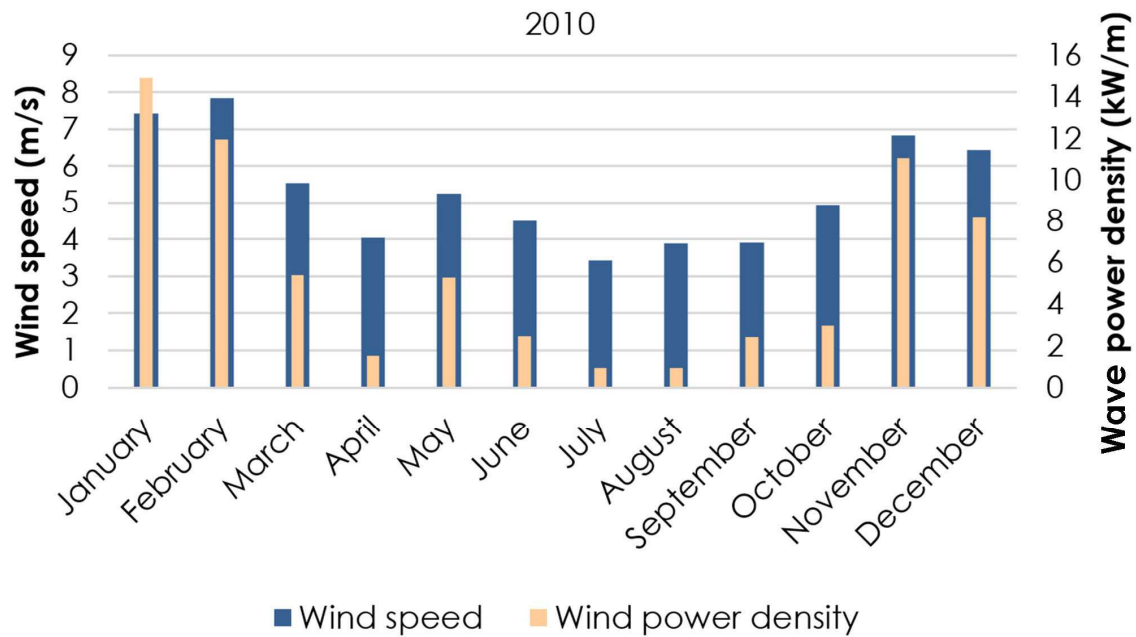


Figure 29: Monthly fluctuation of the available wind velocity and wave potential according to ERA-Interim database at 38°45'N, 14° 45' E [18, 19] for the years 2002, 2005 and 2010.

Finally, the wave potential in the three investigated years seems to follow the same pattern. It is maximized during the winter months, it ranges at medium levels during spring and autumn and it drops considerably during summer.

The wave potential close to the coastline of the island is given by a work accomplished by the Climate Modelling Laboratory of the Italian National Agency for New Technologies, Energy and Sustainable Economic Development, Department of Sustainability [20]. The work was based on a dedicated downscaling of ECMWF data for the Sicilian islands, following specific arithmetic models [21]. The results are presented in Figure 30a for the northern coastline of the island and in Figure 30b for the eastern coastline, regarding the available wave significant height and its direction, given in the form of wave-rose diagrams for each different season of the year.

By comparing these two figures, it is seen that the wave potential in the northern coastline is significantly higher than in the eastern. Additionally, in both northern and eastern coastline, it is confirmed again that the highest wave potential is concentrated during the winter period, the lower in summer, while an intermediate level is available during spring and autumn. With regard to the wave prevailing direction, this is clearly from the west-northwest for the northern coastline, especially during the period of the highest wave energy content (winter). During summer, the wave direction turns clearly to northwest. For the eastern coastline, the wave direction tends to be parallel to the shore, especially during winter, when it is clearly formulated from the north, while it turns to north-northwest during the rest of the year.

Finally, in Figure 31 the wave potential in the northern (left graph) and eastern (right graph) coastline of Salina is depicted. Specifically, the coloured points' allocation among the graphs' main plot area depicts the wave power density distribution versus the wave period and the wave significant height. It is seen that the highest concentration is found between the curves of 2 kW/m and 5 kW/m. Additionally, the chromatic scale depicts the annual average energy density (in kWh/m), according to the horizontal legend bar at the top of the graphs. The

geographical concentration of the highest wave potential at the northern part of the island is also observed by comparing the two graphs presented in Figure 31.

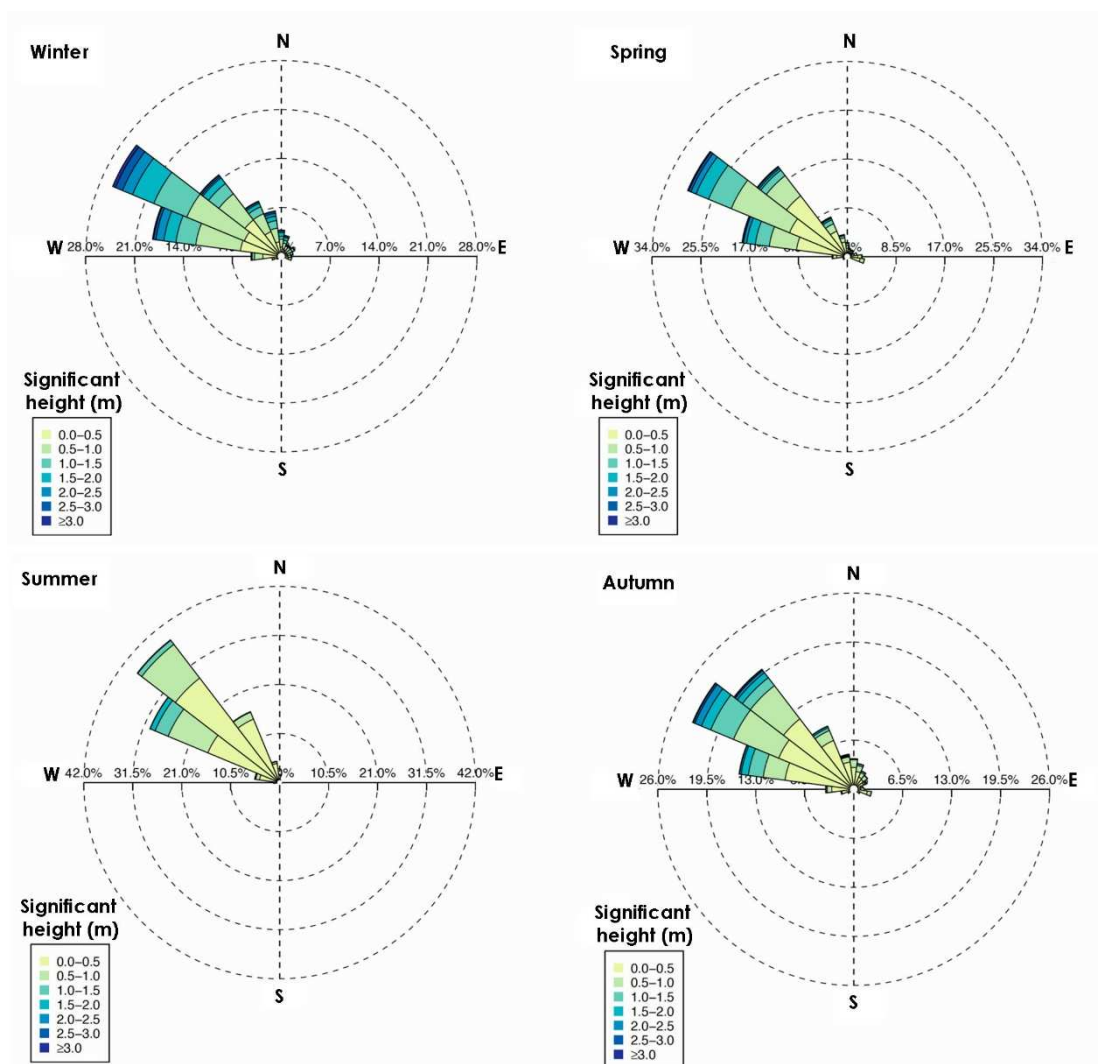


Figure 30a: Available wave significant height in the northern coastline of Salina.

From the above presented and analysed facts and data we come to the conclusion that the under interest area exhibits relatively low wave potential, which on annual average basis can range from 3 to 5 kW/m, despite it is located at the neighbourhood of two of the areas in the Mediterranean Sea which are distinguished among the richest in the basin with regard to the available wave potential (west coast of Sardinia and Sicily).

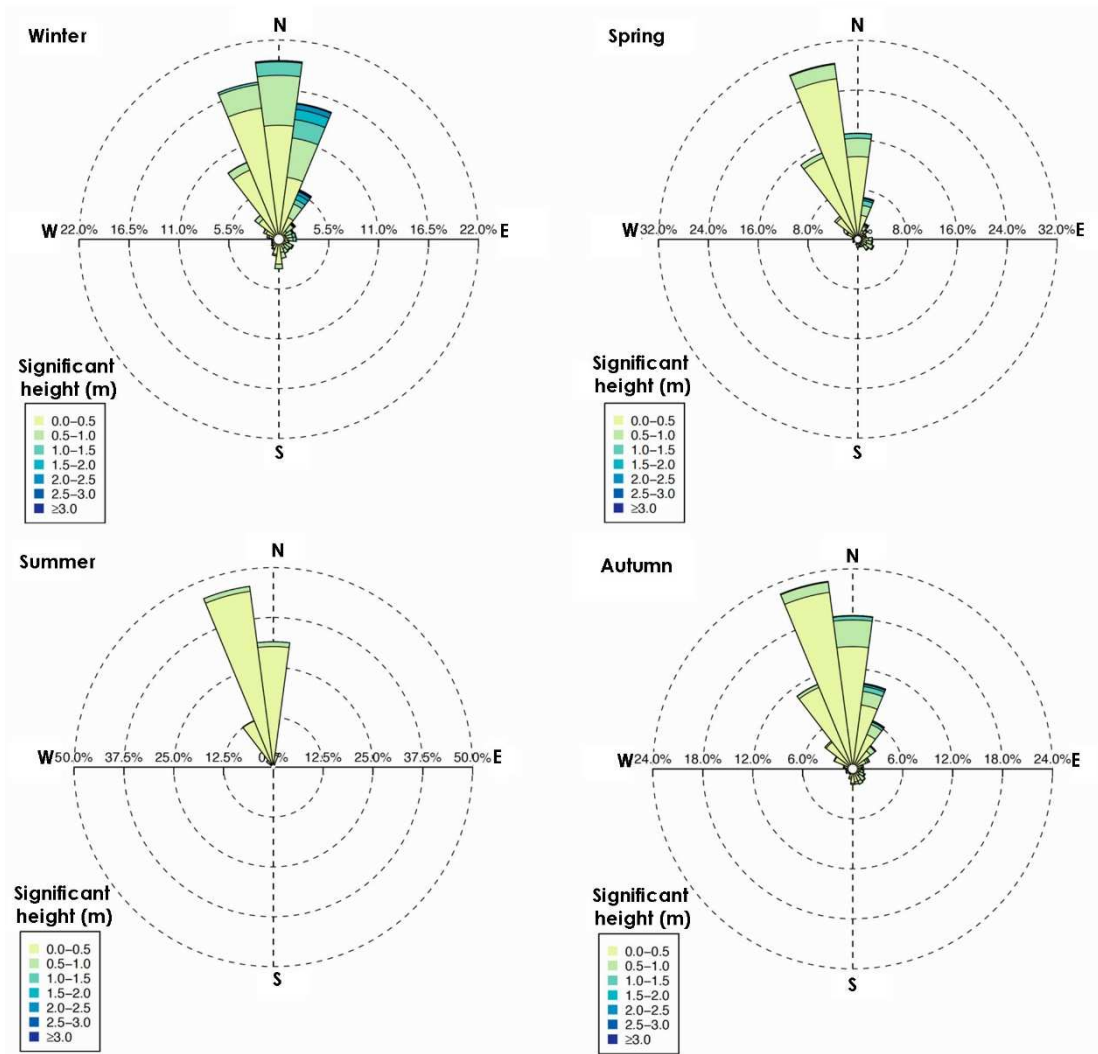


Figure 30b: Available wave significant height in the eastern coastline of Salina.

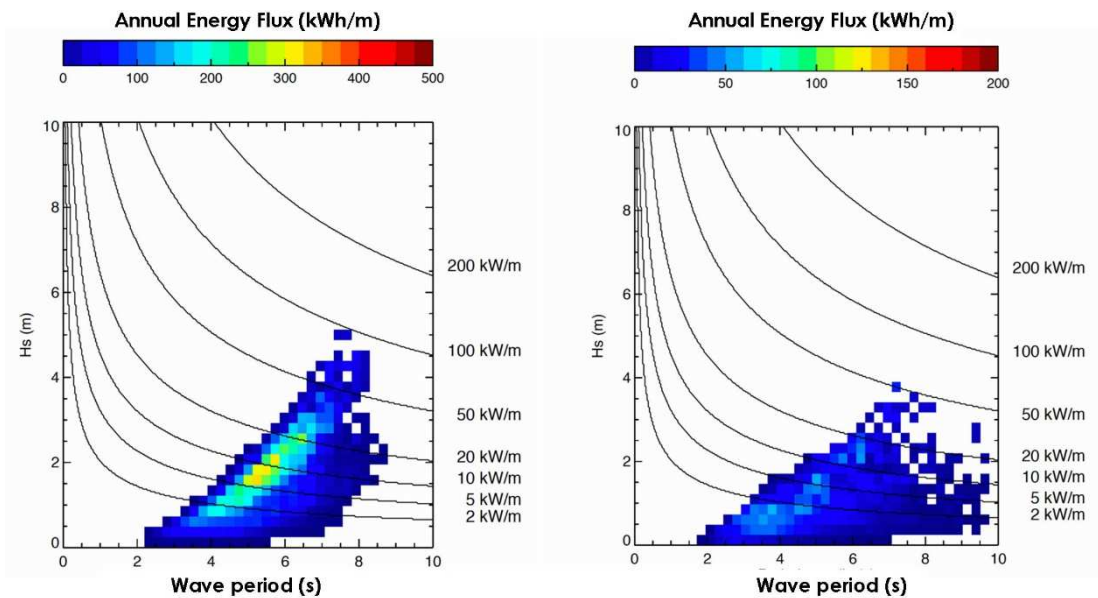


Figure 31: Distribution of the average wave power density and the annual average energy density at the northern (left graph) and the eastern (right graph) coastline of Salina versus the wave period and the wave significant height.

4. Wave Energy Converters

During the last decade it is estimated that, roughly, 100 research projects are running on the investigation of systems, techniques and methods for the development of electricity production projects from wave energy. Over the years, more than 1,000 prototypes have been developed [14]. This fact reveals the conclusion that there is not any technology so far developed on the field of wave energy capturing that can be considered as technically mature and economically competitive. This, in turn, means, that so far there is not any prevailing technology on the wave energy capturing field.

The so far approached systems can be classified in terms of three parameters: the installation location, the size of the Wave Energy Converter (WEC) and the working principle.

Classification versus the installation location

The WECs can be classified versus their installation location as "onshore systems", "nearshore systems" and "offshore systems". This classification is depicted versus their distance from the shore and the available bathymetry in Figure 32 [14].

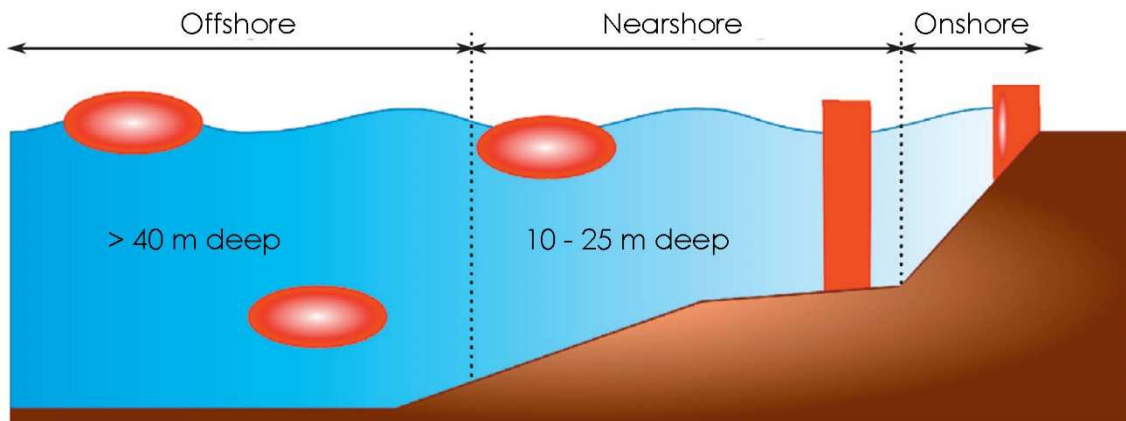


Figure 32: Classification of wave energy converters versus the installation location [14].

Onshore WECs are installed either on shore or very close to the shore, in shallow water, so as in both cases they are either integrated on the shore (e.g. in a breakwater construction, on the rocks etc) or founded on the seabed. It is easily conceived that these systems do not have any requirements for mooring, while, by minimizing their distance from the shore, the maintenance processes are facilitated and the corresponding operating and maintenance costs are minimized. A positive impact on the set-up cost comes also from the reduced required lengths of the interconnection cables, another positive consequence of the vicinity of these systems with the shore. The main disadvantage of onshore WECs is the, sensibly, reduced wave potential close to the shore, due to the influence of the bathymetry on the wave energy content. Another issue may come from any potential environmental impacts, since the shore is reshaped.

Nearshore devices are usually installed a few hundred meters from the shore and in relatively low depths, between 10 m and 25 m. They can be either floating devices or fixed on the seabed. Normally they exploit higher wave potential than onshore systems, while their relatively short distance from the shore enables easier maintenance and approaches higher availability.

Offshore devices are installed in long distances from the shore and in depths higher than 40 m. Their installation position in the open sea creates the conditions for the exploitation of high wave potential, which can be at the range of some tens of kW/m of wave crest. At the same time, their distance from the shore and their exposure to high mechanical loads make their maintenance more demanding and affect their survivability. The set-up cost is also increased due to the long required interconnection cables.

Classification versus the device size and the directional wave characteristics

Versus the device size and the directional characteristics of the wave versus the orientation of the device, the WECs can be distinguished as “attenuators”, “point absorbers” and “terminators”.

Attenuators

The attenuators are long WECs with respect to the wave length, placed in parallel lines with regard to the wave's direction. They consist of a series of cylindrical components, connected together with flexible hinged joints, which enable the rotational motion of each cylinder around the axes of these joints. In this way, each cylinder can perform this rotational motion independently with its neighbouring cylinders, attenuating, in a sense, the wave's amplitude. The operation concept and the constructive structure of an attenuator WEC are graphically presented in Figure 33.

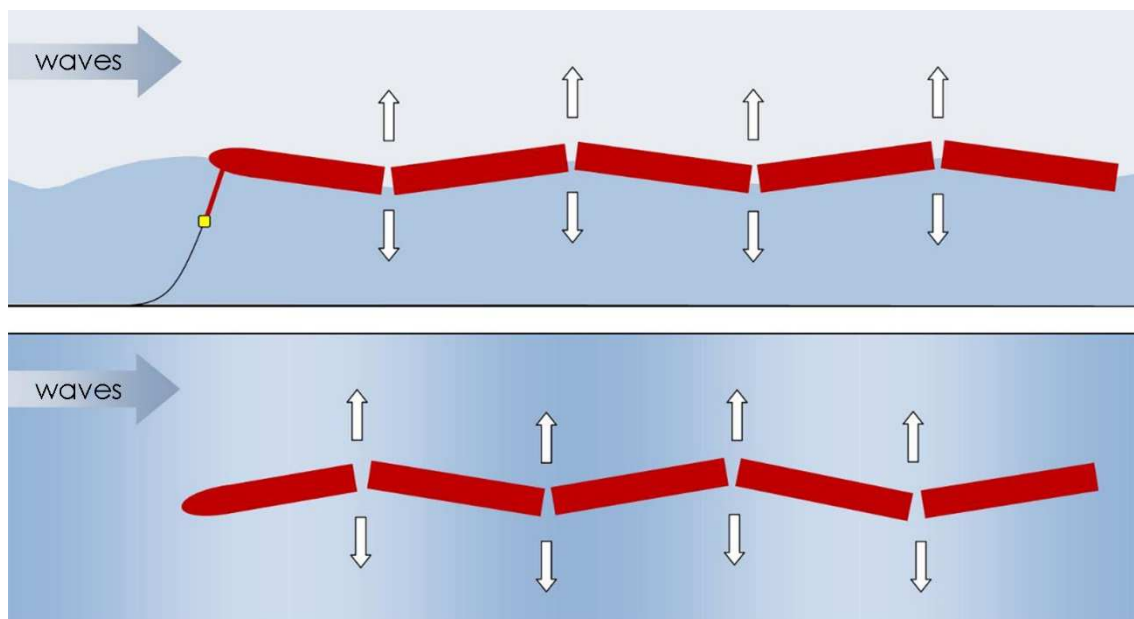


Figure 33: Operation concept and the constructive structure of an attenuator WEC [22].

A quite famous project of this type is the so-called “Pelamis” project, installed in 2008 in the northern Portuguese coast. It is a snake-like slack-moored articulated structure. It consists of four cylindrical sections connected with hinged joints and aligned with the wave direction. The wave induced motion of these joints is resisted by hydraulic rams, which pump high-pressure oil through hydraulic motors driving three electrical generators. Gas accumulators provide some energy storage. Each developed prototype unit has a length of 120 m and a diameter of 3.5 m. The total power output is 750 kW. The Portuguese project is composed of three Pelamis (Figure 34).



Figure 34: The Pelamis devices in the north Portuguese coast [23].

Point absorbers

The point absorbers could be considered as pointwise devices, in the sense that they do not have a dominating dimension with regard to the others. In other words, their horizontal dimensions are much smaller than the wavelength. In this way they are capable to capture wave energy regardless the wave's direction. The electricity is produced by exploiting the bobbing or the pitching action of a device, through which the up and down motion of the wave is converted into rotational or reciprocating movements inside the device, depending on the involved mechanism at each alternative prototype. The point absorbers can be floating or fully sub-merged devices, as shown in Figure 35 [24]. A typical device of this category is the OPT's PowerBuoy with a nominal power of 150 kW, which will be also presented later.

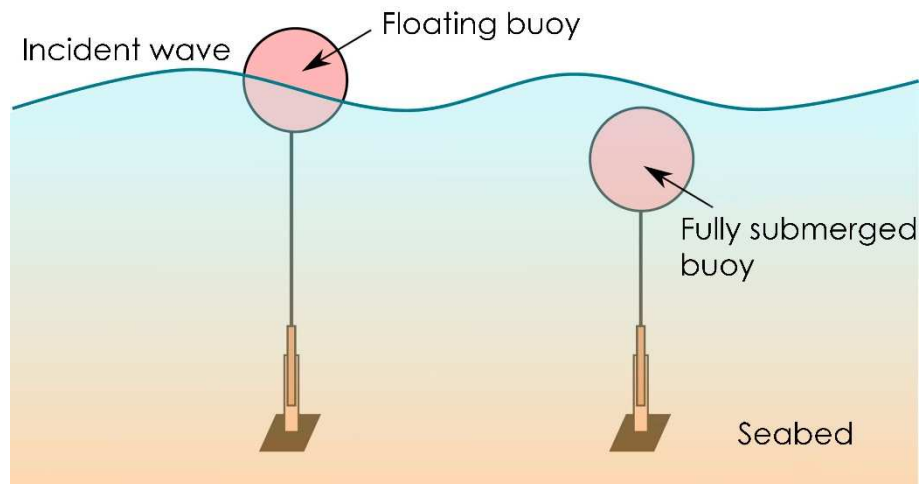


Figure 35: Operation concept and the constructive structure of an point absorber WEC [24].

Terminators

The terminators are WECs placed perpendicular to the wave direction, unlike attenuators. In a sense they terminate the waves' action. A prototype example of this category is the Wave Dragon devices, presented in Figure 36 [25].

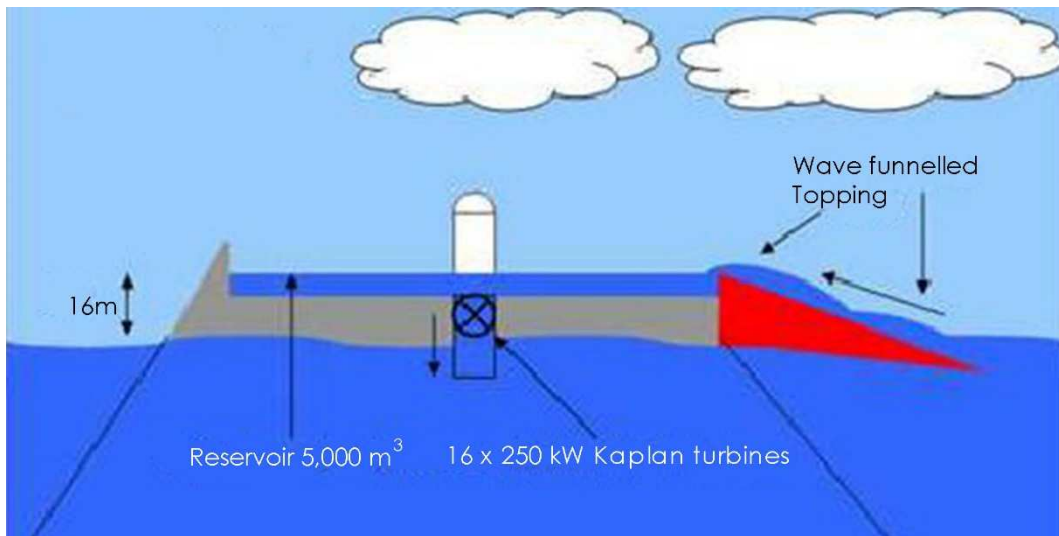


Figure 36: Operation concept and the constructive structure of a terminator WEC [25].

Classification versus the working principle

Finally, the WECs are classified versus the working principle as “pressure differential”, “floating structures”, “overtopping devices” and “impact devices”.

Pressure differential devices

Pressure differential devices can be divided in two sub-categories, the Archimedes Wave Swing (AWS) converters and the Oscillating Water Column (OWC) converters. In the first category of devices, a fully submerged point absorber, typically located near the shore, is fixed in the seabed. Inside the point absorber there is air sealed in an appropriately formulated chamber. The operation principle of the device is based on the pressure difference inside the air chamber as the device changes position below the periodically moved wave's crests and troughs. When there is a wave crest above the device, the pressure of the air inside the device increases, forcing the device to move downwards. During a trough passage above the device, the pressure inside the air chamber drops, enabling the device to move upwards. This up and down motion of the wave converter is transformed to electricity with a linear generator. The overall operation principle and constructive layout are presented in Figure 37 [26].

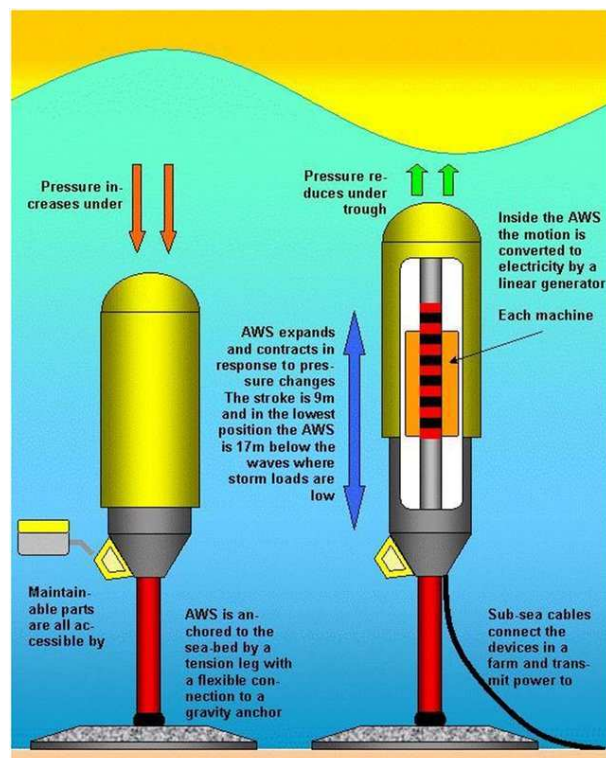


Figure 37: Operation concept and the constructive structure of a AWS converter [26].

The Oscillating Water Column converters are structures usually integrated on the shore or fixed on the seabed. Practically they exploit the same as with the ASW systems principle. The whole system is formulated by a fixed structure, constructed in most cases with concrete, mounted on the coast line. This structure is closed above the sea surface and open below it, with its

front, vertical surface partially submerged. The wave motion forces the sea surface inside the construction to move continuously upwards and downwards. In this way, the air inside the chamber is compressed and decompressed following a circular, periodic pattern, forcing an air turbine, properly located on shore, to perform a continuous rotational motion, always at the same rotating direction, despite the bidirectional air flow through the turbine. The operating principle and the constructive layout of this technology are presented in Figure 38 [27].

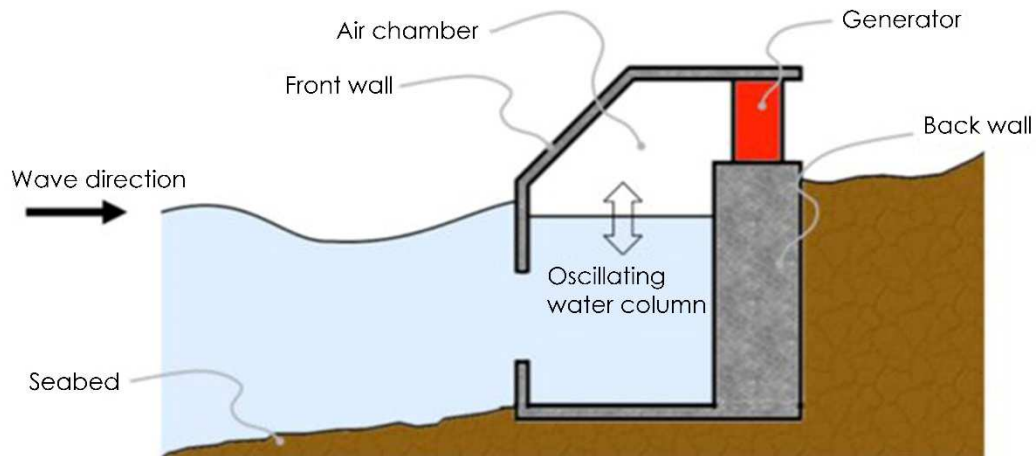


Figure 38: Operation concept and the constructive structure of a OWC converter [27].

Fixed-structured OWC systems have been built in several locations, such as in Toffestallen, Norway (near Bergen) in 1985, in Sakata, Japan in 1990, in Vizhinjam, India (near Trivandrum, Kerala state) in 1990, in Pico Island, in the Azores, Portugal, in 1999 and in Islay Island, Scotland, in 2000 (the LIMPET plant). The largest project ever constructed of this type, named OSPREY, a sea bed mounted system, was set-up in Scotland in 1995, yet it was destroyed by the strong waves soon after its installation and was sunk close to the Scottish coastline. In all these implemented projects, the structure was constructed with concrete, apart from the OSPREY project. The vertical cross-sectional area of the interior space in these space, estimated by accounting an average level of the sea surface, ranges from 80 m² to 250 m². The nominal electrical power output of these implemented projects was from 60 kW to 250 kW, apart from OSPREY, which had a power output of 2 MW.

A novelty of these systems lays on the extension of the interior air chamber by protruding vertical walls, perpendicular to the waves' direction. In this way, the wave energy capturing process is enhanced. Such a system was constructed in Port Kembla, Australia, in 2005 (Figure 39).



Figure 39: The sea bed mounted, fixed-structure OWC project in Port Kembla, Australia [28].

Civil works, namely the fixed-structured construction, exhibits the major impact on the total set-up cost of fixed OWC systems. An approach to relieve this impact is through the integration of the civil works with breakwater constructions. In this way, the construction costs are shared, while easy and secure accessibility to the system is ensured, affecting positively the required maintenance cost. Such constructions have been adopted in Sakata, Japan in 1990, where one of the caissons utilized for the formulation of the breakwater has been properly shaped to host the mechanical and electrical equipment of the OWC system (Figure 40). Similar approaches have been also introduced in mouth of Douro river in Portugal and at the port of Mutriku, in northern Spain.



Figure 40: The fixed-structure OWC project in Sakata, Japan, mounted on the breakwater [28].

The main concept of the floating pressure differential systems is depicted in Figure 41, entitled as the Backward Bent Duct Boy (BBDB). With the BBDB structure, the WECs duct is placed backward, with regard to the wave incident direction. This formulation has been proved to be more effective with regard to the wave energy exploitation. With the BBDB layout, the height of the water column inside the air chamber can be adequately large, while the draught of the floating structure is maintained within acceptable limits.

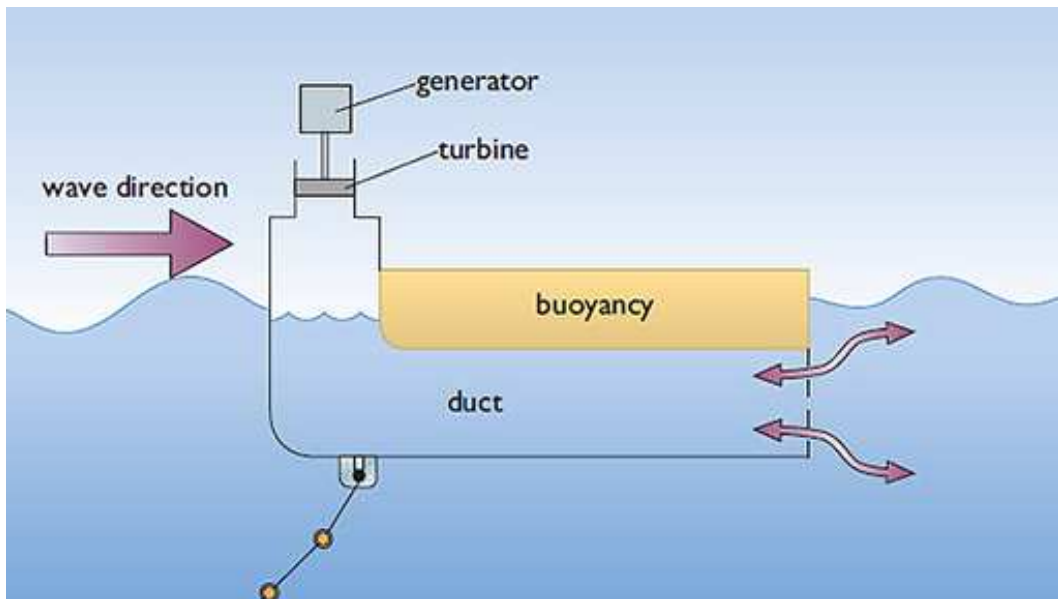


Figure 41: The constructional and operation concept of the Backward Bent Duct Boy [29].

Another typical project in this category is the Mighty Whale, developed by the Japan Marine Science and Technology Center. It consists of a floating structure (length 50 m, breadth 30 m, draught 12 m, displacement 4400 tn), with three air chambers located at the front, side by side, and buoyancy tanks, equipped with Wells air turbines (Figure 42). The total nominal power is 110 kW. The device was placed near the mouth of Gokasho Bay, in Mie Prefecture, Japan, in 1998.

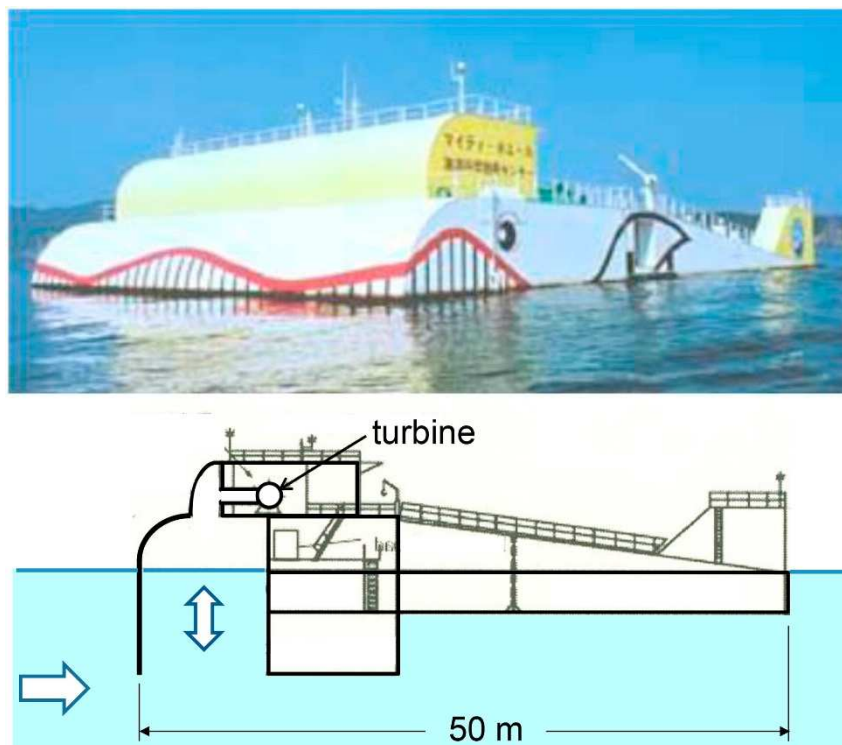


Figure 42: The Mighty Whale floating OWC [28].

Floating structures

Floating structures are based on a floating body which exploits any possible movement of the waves, namely any horizontal or vertical or pitch or any combination of them motion. The

motion of the floating device can be the absolute motion with regard to a fixed, steady point, e.g. at the seabed, or the relative motion with regard to another fully submerged body.

The simplest devices of oscillating body systems are the single-body heaving buoys. These devices consist of a buoy at the sea surface connected to the power generation system, fixed at the sea bottom. The buoy executes an oscillating motion, following the up and down motion of the sea surfaces, which is transmitted in the linear power generation device with a cable which is kept tight with a string or a similar system, as shown in Figure 43. The transmitted oscillating motion of the buoy activates the Power Take-Off mechanism (PTO), which typically consists of a piston pump that supplies with high pressure water a hydraulic turbine.

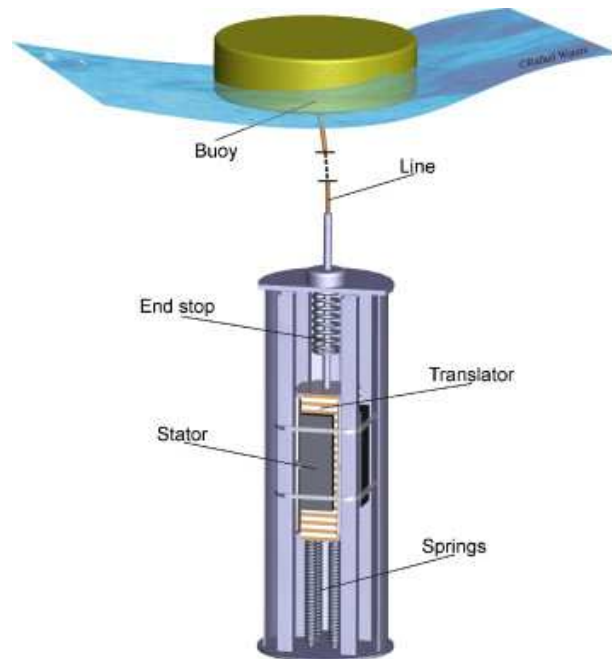


Figure 43: Single-body heaving buoy with linear electrical generator [23].

Single-body heaving buoys may exhibit difficulties associated with the distance between the sea surface and the fixed structure at the sea bottom, as well as any horizontal forces on the vertical construction due to tidal streams. The inconveniences are avoided with two-body heaving systems, in which power is produced due to the relative motion of two floating bodies oscillating differently. A typical system, developed by the Swedish Sven A. Noren, is presented in Figure 44. It consists of a floating buoy which is rigidly connected to a fully submerged vertical tube, open at both ends, known as the “acceleration tube”. The tube contains a piston, whose relative motion with regard to the floating buoy – submerged tube drives a PTO mechanism. With an improved version of the initial prototype, Noren achieved to handle the inadequacies occurred at the end stops of the oscillating piston. This is was done with the configuration of the tube’s edges, inside which the piston slides, in a bell-shape.

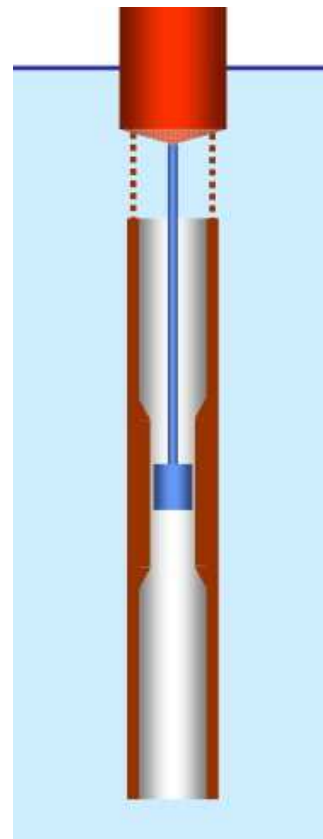


Figure 44: The two-body heaving buoy designed by Sven A. Noren [23].

Typical implemented prototypes of floating structures are the Searaser converter, presented in Figure 45 [30, 31] and the WaveStar, presented in Figure 46 [33].

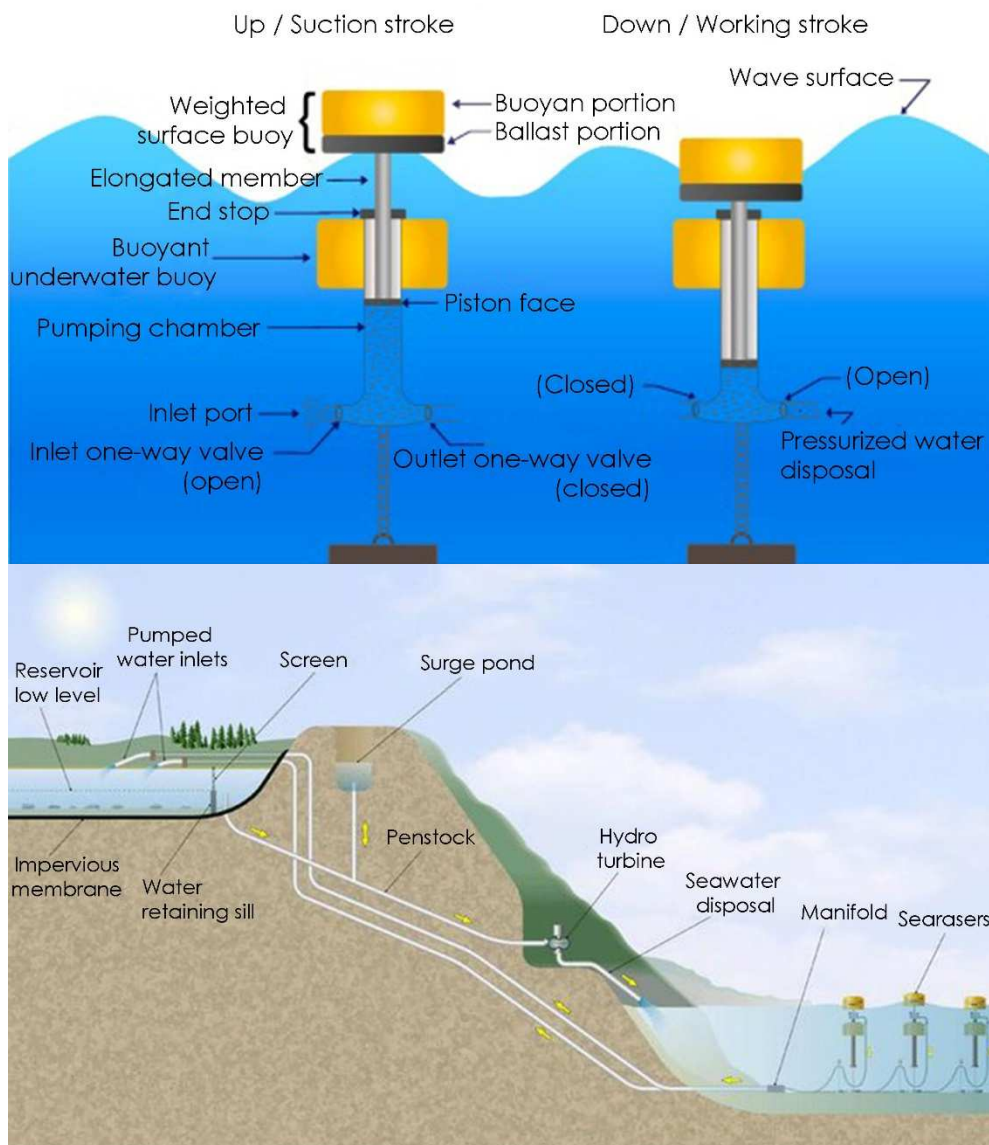


Figure 45: Operation concept and the constructive structure of the Searaser floating converter [30, 31].

The power production in Searaser is accomplished by a vertical piston, which moves up and down, following the motion of the surface buoy and the forces of gravity. The buoy is lifted upwards with wave crests and moves downwards until the cylinder, due to gravity, during the wave troughs, namely under absence of seawater below it. The overall device is held by an anchor fixed on the seabed. The oscillating piston initially lifts seawater to pressurize it during its downwards motion and store it to onshore water reservoirs, in order to be exploited in hydro power plants for electricity generator.

The Wavestar system is a fixed structure, as a unity, since it is steadily fixed with legs secured on the seabed. However, it can be classified as a floating WECs, because the power production is executed by floats that are lifted by the seawater and fall by themselves due to gravity, attached by arms on the overall platform. The up and down oscillating movement of the floats

is transformed via hydraulics into rotational motion, transferred to an inductive generator to produce electricity.

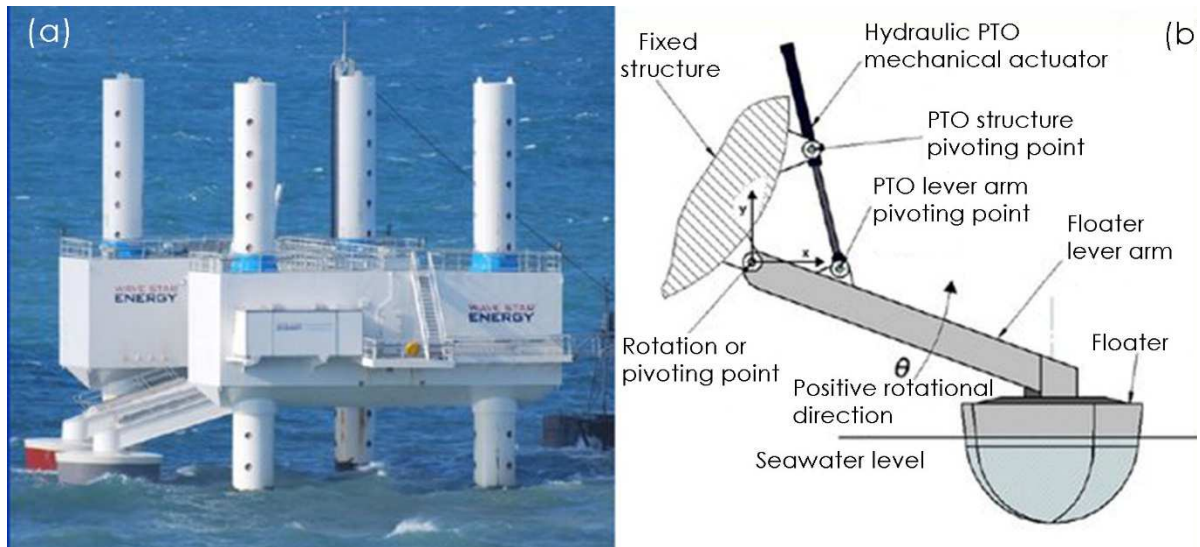


Figure 46: Operation concept and the constructive structure of the WaveStar floating converter [32].

Overtopping systems

Overtopping wave energy converters are floating devices or structures fixed on shore, which force the seawater to pass above them, where it is led through their appropriate configuration to pass through hydro turbines. Practically, these devices base the energy production from the wave potential on the partial transformation of the seawater kinetic energy to potential energy and the exploitation of the combined potential and kinetic energy to mechanical power on the shaft of the involved hydro turbines. In this category the Wave Dragon device presented Figure 37 as a typical terminator system belongs. Wave Dragon systems can exhibit a nominal power of 4 MW to 10 MW, depending on the available wave potential at the installation site. Another typical example of overtopping fixed on shore system is the Sea Slot-cone Generator (SSG) wave energy converter, such as the one implemented on Kvitsoy, Norway [33]. Typical configuration of a SSG wave converter is shown in Figure 47 [34].

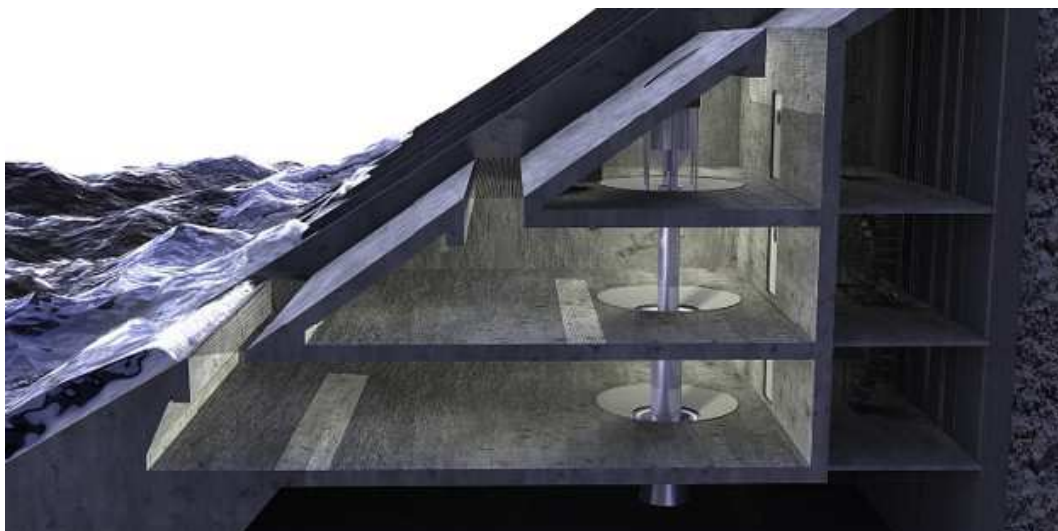


Figure 47: Operation concept and the constructive structure of the SSG wave energy converter [34].

As seen in Figure 47, the overall structure is formulated with several reservoirs placed on different levels with regard to the sea surface and the one at the top of the other, in a ladder-pattern. Seawater enters these reservoirs, as lifted while the waves strike the shore, and stored in the form of potential energy. The captured seawater flows through vertical axis hydro turbines. Seawater is recirculated back to the sea from the hydro turbines' outlet, located on the rear part of the overall construction. The construction layout of the SSG system enables operation under a wide range of wave conditions, maximizing the system's overall efficiency.

Impact devices

Finally, the impact devices are formulated by an articulated or flexible structure, which is positioned perpendicular to the wave direction, forcing a deflector to move forward to backward, due to the wave's impact. This motion is transformed to air pressure through a reciprocating motion, which is transferred to a pressurized water pipeline. Eventually, the under pressure water is led to hydro turbines, located on shore, where electricity is generated, typically as in common hydro power plants. The overall concept of these devices is shown in Figure 48 [35]. Specifically, in this figure the implemented project of Aquamarine Power Oyster is presented, with a nominal power of 800 kW. These devices are also known as Oscillating Wave Surge (OWS) converters.

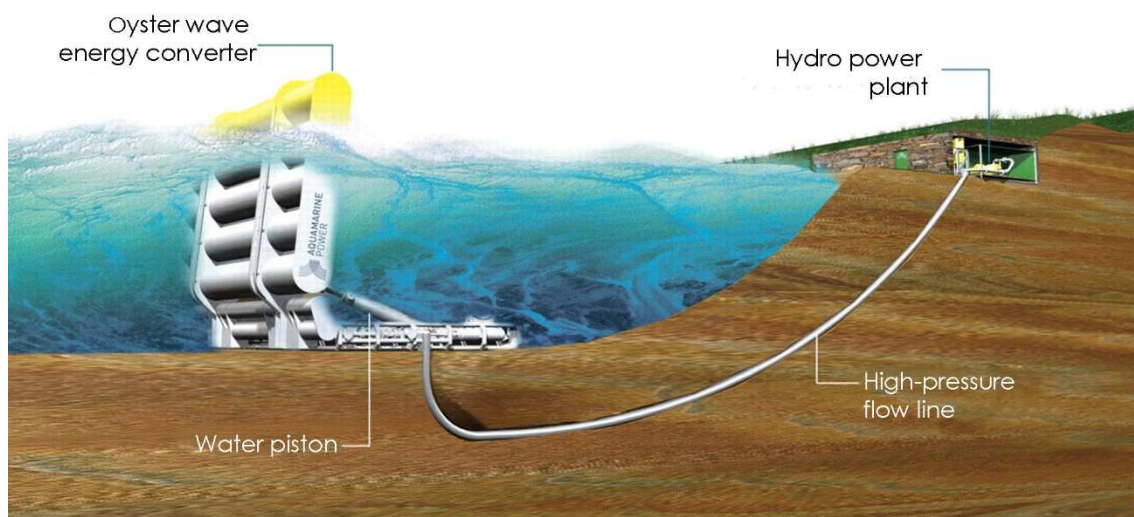


Figure 48: Operation concept and the constructive structure of th an impact wave energy converter [35].

According to the European Marine Equipment Centre, in 2013 there were 157 WEC concepts designed and developed. More than 50% of them are located in Europe, with the United Kingdom being the main developer country [36]. A common feature of all the so far developed technologies is that all of them are in early stage and there is no-one outweighing over the others. Yet, as shown in Figure 49, it seems that developers exhibit a clear tendency to develop point absorber systems, rather than other types of WECs. Most probably, this is because these systems are less expensive and complex than the other proposed technologies [14].

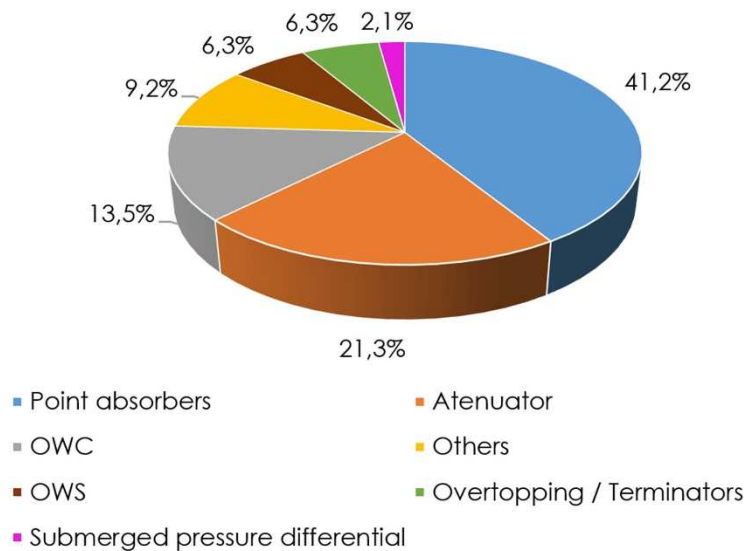


Figure 49: Global percentage share of alternative WECs technologies [14].

Additionally, Marine Energy Matters has proposed the following seven stages regarding the Technology Readiness Level of WECs [37]:

- TRL1: Concept release
- TRL2: Concept validated by a University or an Engineering Research Organisation
- TRL3: Tank testing (scale device)
- TRL4: Location testing (scale device)
- TRL5: Full large scale grid connected prototype
- TRL6: Pre-commercial, grid connected array
- TRL7: Fully certified, by a recognized certification body, commercial array.

According to Marine Energy Matters, only 5% of the so far developed WECs have reached TRL5. Most concepts have been developed until TRL3, because until this stage the required amounts are relatively low. The transition from TRL4 to TRL5, namely from the Lab to real sea conditions, is the most difficult and the slowest progress, since it imposes difficult technical issues and costly processes.

Conclusions

Following the results of the above presented analysis, we could come to the following conclusions:

- The examined area is not characterized with rich wind or wave potential.
- The low wave potential combined with the considerably high set-up cost of the available wave energy technologies does not create favourable conditions for the exploitation of wave energy in the island of Salina. This approach does not seem to be economically feasible.
- The only feasible solution among the investigated systems in this study, towards energy transition in Salina, is the introduction of offshore wind parks. However, it should be noted that even with this technology, the low available wind potential implies annual capacity factors lower than 20%. These values, sensibly, impose respectively reduced economic efficiency of the required investment. The economic feasibility of the project will be configured, apart from the capacity factor of the offshore wind park, by the produced electricity selling price, any probable wind power curtailments due to grid security and stability reasons and the potential availability of a subsidy on the project's set-up cost.
- The electricity production specific cost from wave energy converters, in general, is estimated at 0.12 to 0.44 €/kWh [14]. Additionally, for offshore wind parks, the same feature is given from 0.14 to 0.46 €/kWh [38]. Normally, for the case of Salina, the expecting annual electricity production cost from either wave energy converters or offshore wind parks should be closer to the higher limits of the above presented ranges, due to the low to moderate available wave or wind potential. This, of course, will affect the margin for low selling price of the produced electricity.

To conclude with, the achievement of high Renewable Energy Sources (RES) penetration in Salina does not seem to be an easy task. The process is not obvious, since all the available technologies should be involved, starting with energy saving technologies in buildings, hotels etc, aiming at the maximum possible saving on electricity consumption, and ending with the introduction of electricity and thermal energy production technologies from RES in the optimum synthesis (wind parks, photovoltaics, solar collectors), following the results of a relevant feasibility study.

References

- [1] Wikipedia: Salina, Sicily: https://en.wikipedia.org/wiki/Salina,_Sicily. (accessed on October 2019).
- [2] Greek Directive on Buildings' Energy Performance. Official Governmental Gazette 2367B' /12-7-2017.
- [3] European Centre for Medium-Range Weather Forecasts (ECMWF): ERA5 from the Copernicus Climate Change Service (C3S) Climate Data Store. <https://cds.climate.copernicus.eu/#!/search?text=ERA5&type=dataset> (accessed on December 2019).
- [4] EMODnet: Understanding the Bathymetry of the European Seas: <https://portal.emodnet-bathymetry.eu/> (accessed on September 2019).
- [5] N. Khan, A. Kalair, N. Abas, A. Haider. Review of ocean tidal, wave and thermal energy technologies. *Renewable and Sustainable Energy Reviews* 2017; 72: 590 – 604.
- [6] Meyers RA, editor. *Encyclopedia of Sustainability Science and Technology*. New York, NY: Springer New York; 2012. doi: 10.1007/978-1-4419-0851-3.
- [7] McCormick ME. *Ocean wave energy conversion*. New York: Wiley; 1981.
- [8] Ross D. *Power from sea waves*. Oxford: Oxford University Press; 1995.
- [9] Tricker RAR . *Bores, breakers, waves and wakes: an introduction to the study of waves on water*, 1st ed. Mills & Boon; 1964.
- [10] Wikipedia: Wind wave. https://en.wikipedia.org/wiki/Wind_wave (accessed on December 2019).
- [11] Fleming A, Penesis I, Macfarlane G, Bose N, Denniss T. Energy balance analysis for an oscillating water column wave energy converter. *Ocean Engineering and Marine Research* 2012; 54: 26–33. <http://dx.doi.org/10.1016/j.oceaneng.2012.07.002>.
- [12] Cornett V. A global wave energy resource assessment. In: *International offshore and polar engineering conference (ISOPE)*, vol. 1, 2008. p. 318-26.
- [13] Reguero B, Vidal C, Menendez M, Mendez F, Mínguez R, Losada I. Evaluation of global wave energy resource. In: *OCEANS*, 2011. p.1–7.
- [14] Iraide López, Jon Andreu, Salvador Ceballos Iñigo Martínez de Alegría, Iñigo Kortabarria. Review of wave energy technologies and the necessary power-equipment. *Renewable and Sustainable Energy Reviews* 2013; 27: 413-434.
- [15] Mork G, Barstow S, Kabuth A, Pontes M. Assessing the global wave energy potential. In: *International conference on ocean, offshore mechanics and arctic engineering (OMAE)*, vol. 20473, 2010. p. 447–54.
- [16] Luca Liberti, Adriana Carillo, Gianmaria Sannino. Wave energy resource assessment in the Mediterranean, the Italian perspective. *Renewable Energy* 2013; 50: 938-949.
- [17] G. Besio, L. Mentaschi, A. Mazzi. Wave energy resource assessment in the Mediterranean Sea on the basis of a 35-year hindcast. *Energy* 2016; 94: 50-63.
- [18] Dee, D. P., Uppala, S. M., Simmons, A. J., Berrisford, P. , Poli, P. , Kobayashi, S. , Andrae, U. , Balsameda, M. A., Balsamo, G. , Bauer, P. , Bechtold, P. , Beljaars, A. C., van de

- Berg, L. , Bidlot, J. , Bormann, N. , Delsol, C. , Dragani, R. , Fuentes, M. , Geer, A. J., Haimberger, L. , Healy, S. B., Hersbach, H. , Hólm, E. V., Isaksen, L. , Kållberg, P. , Köhler, M. , Matricardi, M. , McNally, A. P., Monge-Sanz, B. M., Morcrette, J. , Park, B. , Peubey, C. , de Rosnay, P. , Tavolato, C. , Thépaut, J. and Vitart, F. The ERA-Interim reanalysis: configuration and performance of the data assimilation system. *Quarterly Journal of the Royal Meteorological Society* 2011; 137: 553-597. doi:10.1002/qj.828.
- [19] ECMWF: ERA Interim Daily: <https://apps.ecmwf.int/datasets/data/interim-full-daily/levtype=sfc/> (accessed on December 2019).
- [20] Italian National Agency for New Technologies, Energy and Sustainable Economic Development, Department of Sustainability: <https://impatti.sostenibilita.enea.it/en> (accessed on December 2019).
- [21] Climate Modelling Laboratory of the Italian National Agency for New Technologies, Energy and Sustainable Economic Development, Department of Sustainability: Report on Wind and Wave Potential on the Islands of Ginostra, Lipari and Salina.
- [22] Mohd Farriz Basar, Azhan Ab. Rahman, Asri Din, Muhammad Sharil Yahaya and Zubir Mahmud. Design and Development of Green Electricity Generation System Using Ocean Surface Wave. PEA-AIT International Conference on Energy and Sustainable Development: Issues and Strategies (ESD 2010) The Empress Hotel, Chiang Mai, Thailand. 2-4 June 2010.
- [23] António F. O. Falcão. Wave energy utilization: A review of the technologies. *Renewable and Sustainable Energy Reviews* 2010; 14: 899-918.
- [24] N. Y. Sergiienko, B. S. Cazzolato, B. Ding, P. Hardy, M. Arjomandi. Performance comparison of the floating and fully submerged quasi-point absorber wave energy converters. *Renewable Energy* 2017; 108: 425-437.
- [25] Andreas Poullikas. Technology prospects of wave power systems. *Electronic Journal of Energy and Environment* 2014; Published online 30 April 2014 (www.ejee.cl). DOI 10.7770/ejee-V2N1-art662.
- [26] Jonathan Blackledge, Eugene Coyle, Derek Kearney, Ronan McGuirk and Brian Norton. Estimation of Wave Energy from Wind Velocity. *Engineering Letters* 2013; 21:4, EL_21_4_01
- [27] R. Vertechy, M. Fontana, G.P. Rosati Papini, M. Bergamasco. Oscillating-water-column wave-energy-converter based on dielectric elastomer generator. *Proceedings of SPIE - The International Society for Optical Engineering* · April 2013. DOI: 10.1117/12.2012016.
- [28] António F. O. Falcão, João C. C. Henriques. Oscillating-water-column wave energy converters and air turbines: A review. *Renewable Energy* 2016; 85: 1391-1424.
- [29] OpenLearn: Can renewable energy sources power the world? https://www.open.edu/openlearn/ocw/mod/oucontent/view.php?id=73764&extra=thumbnailfigure_idp5702832 (accessed on September 2019).
- [30] Tanvir Shahriar, M. Ahsan Habib, M. Hasanuzzaman, M. Shahrear-Bin-Zaman. Modelling and optimization of Searaser wave energy converter based hydroelectric power generation for Saint Martin's Island in Bangladesh. *Ocean Engineering* 2019; 192: 106289.

- [31] Aliakbar Babajani. Hydrodynamic Performance of a Novel Ocean Wave Energy Converter. *American Journal of Fluid Dynamics* 2018, 8: 73-83. DOI: 10.5923/j.ajfd.20180803.01.
- [32] Francesco Ferri 1, Simon Ambuhl, Boris Fischer, Jens Peter Kofoed. Balancing Power Output and Structural Fatigue of Wave Energy Converters by Means of Control Strategies. *Energies* 2014; 7: 2246-2273; doi: 10.3390/en7042246.
- [33] Vicinanza D, Margheritini L, Kofoed J P, Buccino M. The SSG wave energy converter: performance status, and recent developments. *Energies* 2012; 5 (2):193–226.
- [34] L. Margheritini, D. Vicinanza, P. Frigaard. SSG wave energy converter: Design, reliability and hydraulic performance of an innovative overtopping device. *Renewable Energy* 2009; 34:1371-1380.
- [35] Yanji Wei, Ashkan Rafiee, Alan Henry, Frederic Dias. Wave interaction with an oscillating wave surge converter, Part I: Viscous effects. *Ocean Engineering* 2015; 104: 185-203.
- [36] European Marine Equipment Centre: <http://www.emec.org.uk/> (accessed on December 2019).
- [37] Marine energy, global development review 2011, private limited company 06746222, Marine Energy Matters, Cleaveland House 1 Cleaveland Rise, East Ogwell, Newton Abbot, Devon, TQ12 6FF; 2011.
- [38] Röckmann C., Lagerveld S., Stavenuiter J. (2017) Operation and Maintenance Costs of Offshore Wind Farms and Potential Multi-use Platforms in the Dutch North Sea. In: Buck B., Langan R. (eds) *Aquaculture Perspective of Multi-Use Sites in the Open Ocean*. Springer, Cham.



Published by the
Clean Energy for EU Islands Secretariat



© European Union

This publication does not involve the European Commission in liability of any kind.